John Firestone

Resolving the Younger Dryas Event through Borehole Thermometry

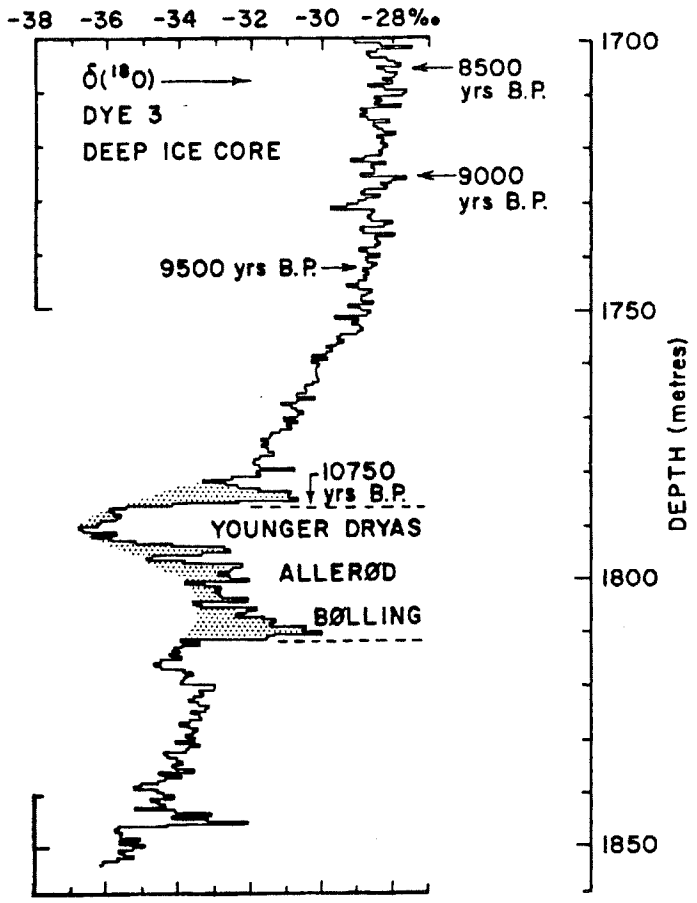

PH.D. DISSERTATION • GEOPHYSICS PROGRAM • UNIV. OF WASHINGTON

John Firestone

Resolving the Younger Dryas Event through Borehole Thermometry

A dissertation submitted in partial fulfillment
of the requirements for the degree of

Doctor of Philosophy

University of Washington
Geophysics Program

1992

Chairman of the Supervisory Committee
EDWIN WADDINGTON

Copyright © 1992 by John Firestone
Second printing with corrections 1992
93 92 4 3 2

The cover illustration and the following figures have been reprinted with permission from copyrighted works: Figures 1.1, 1.4, and 1.7 with permission from the authors and Nature, Copyright © 1985, 1989 Macmillan Magazines Ltd., London; Figures 1.2 and 1.3 with permission from the authors and Geochemica et Cosmochimica Acta, Copyright © 1989, Pergamon Press Ltd, Oxford; the cover illustration and Figure 1.5 with permission from the authors and the Geological Society of America, Copyright © 1987, Geological Society of America, Boulder, Colorado; Figures 1.6 and 2.1 with permission from the authors and the American Geophysical Union, Copyright © 1985, 1990, American Geophysical Union, Washington, D.C.

Sparcstation is a trademark of Sun Microsystems, Incorporated.

In presenting this dissertation in partial fulfillment of the requirements for the Doctoral degree at the University of Washington, the author agrees that the University of Washington Library shall make its copies freely available for inspection. The author further agrees that extensive copying of this dissertation is allowable only for scholarly purposes consistent with "fair use" as prescribed in the U.S. Copyright Law. Requests for copying or reproduction of this dissertation may be referred to University Microfilms, 1490 Eisenhower Place, P.O. Box 975, Ann Arbor, MI 48106, to whom the author has granted "the right to reproduce and sell (a) copies of the manuscript in microfilm and/or (b) printed copies of the manuscript made from microfilm."

Copies of this dissertation with corrections are available from the author, c/o the Geophysics Program AK-50, University of Washington, Seattle, WA 98195.

Printed in the United States of America
Set in Gill Sans and ITC New Baskerville

Contents

APPENDICES

Figures

Tables

Acknowledgments

I would like to thank Edwin Waddington for his patient guidance and support while I worked on this project and tested many untried ideas. The members of my supervisory committee, Pieter Grootes, Douglas MacAyeal, and Charles Raymond offered many constructive comments and thoughtful suggestions in the research and preparation of this opus. Stephen Warren helped me in many ways in my first few years of graduate school.

I would also like to thank the staff of the Geophysics program for guiding me past the tar pits of academia and providing an agreeable environment for research. My office mates and fellow students can not escape mention for their help and conversation leading to many stimulating and occasionally iconoclastic ideas.

I had the pleasure of visiting the University of Copenhagen for a few weeks during this project. I wish to thank, in particular, Dorthe Dahl-Jensen, Bjarne Andreson, Niels Gundestrup, Christine (Schøtt) Hvidberg, and Jacob Pederson for helpful discussions and cheerful hospitality.

Finally, I wish to express my deep gratitude to my friends and family for their encouragement and unflagging support.

❄

Temperature data used in this work were graciously provided by Niels Gundestrup. Oxygen isotopic data were supplied by the World Data Center A for Glaciology, Boulder, Colorado. Christine (Schøtt) Hvidberg kindly provided Summit model velocities. The cover illustration, Figures 1.1–1.7, and Figure 2.1 have been reproduced from copyrighted sources, with the kind permission of the authors and publishers.

Funding for this work was provided by the University of Washington Geophysics Program (Ronald Merrill, chairman) and by the National Science Foundation under grants DPP 8613935, DPP 891498, DPP 8915924, and DPP 9024098.

Abstract

One of the most striking features of the ice core records from Greenland is a sudden drop in oxygen isotope values (delta O-18) between approximately 11 500 and 10 700 years ago. This Younger Dryas event was an intense return to ice age conditions during a time of general deglaciation. As recorded in the ice cores, temperatures in Greenland cooled by roughly seven degrees Kelvin.

W. Broecker and R. Fairbanks have proposed competing explanations for the cooling and cause of this "aborted ice age". One supposes that the seven degree cooling is real and results from a shutdown in the North Atlantic ocean circulation; the other, that it is largely fictitious and records an intrusion of isotopically light glacial meltwater into the ice core records.

Using optimal control methods and heat flow modelling, the author makes a valiant but ultimately futile attempt to distinguish the Younger Dryas event in the ice sheet temperatures measured at Dye 3, South Greenland. The author discusses the prospects for attempting the same in the new Summit boreholes in Central Greenland: how that will require more accurate temperature measurements, a coupled thermo-mechanical model, and a refined uncertainty analysis. He concludes by discussing how borehole temperature analysis may improve the climate histories determined from ice cores.

Common Symbols

(and equations of first use)

(2.7)	A_0	ice flow law constant
(A.12)	$\mathbf{C}$	nodal heat capacities
(2.1)	c	heat capacity
(2.1)	c_1	generic constant
(2.2)	d_{ij}	strain rate tensor
(2.2)	f	internal heat production/ unit volume
(A.12)	$\mathbf{K}$	nodal thermal conductivities
(5.2)	L	performance function
(5.6)	L'	augmented performance function
(4.3/A.18)	m	model parameter index or time step index
(4.3/A.22)	M	number of model parameters - 1 or number of time steps
(A.21)	N	number of spatial nodes
(4.4)	$\tilde{N}$	number of borehole observations
(A.1)	N_i	nodal shape function
(2.7/3.1)	n	ice flow law exponent or observation index
(5.3)	$\mathbf{P}$	flux forcing preconception
(2.7)	Q	activation energy of creep
(A.7)	$\mathbf{Q}$	external nodal heat sources
(5.3)	$\mathbf{Q}_f$	model forcing values
(4.10)	Q_g	geothermal heat flux
(5.2)	$\mathbf{Q}_s$	surface flux forcing
(A.12)	$\mathbf{R}$	internal nodal heat sources
(5.3)	$\mathbf{S}_P$	squared preconception variances
(4.8)	$\mathbf{S}_{\tilde{\Theta}}$	squared observation variances
(2.1)	T	temperature
(A.8)	$\mathbf{T}$	nodal temperatures
(A.12)	$\dot{\mathbf{T}}$	time change in the nodal temperatures
(A.23)	$\tilde{\mathbf{T}}$	terminal nodal temperatures
(4.10)	$\mathbf{T}_s$	surface temperature history
(2.1)	t	time
(2.6)	u	horizontal velocity
(2.9)	$\hat{u}(z)$	horizontal velocity profile
(2.6)	w	vertical velocity
–	$w(sfc)$	vertical surface velocity
(2.6)	x	horizontal flow line direction
(2.6)	y	horizontal direction transverse to the flow line
(2.6)	z	vertical direction
(2.1)	ρ	material density
(2.1)	K	thermal conductivity
(3.1)	χ^2	statistical chi-squared value
(A.16)	Δt	time step size
(5.12)	δ_{ij}	Kronecker delta
(5.6)	λ	adjoint trajectory
(2.2)	σ_{ij}	deviatoric stress tensor
(3.1)	σ_n	observation/preconception variances
(3.1)	Θ	synthetic temperature observations
(4.4)	$\tilde{\Theta}$	borehole temperature observations

Part One

CHAPTER ONE

The Younger Dryas Problem

One of the most striking features of the ice core records from Greenland is a series of large and rapid oscillations in oxygen isotope values ($\delta^{18}O$) over the last glaciation. From comparisons of present day $\delta^{18}O$ values in Greenland and Antarctica with mean annual temperatures (Picciotto 1960; Lorius *et al.* 1968; Dansgaard *et al.* 1973), these oscillations suggest that the air temperature over Greenland went through episodes of rapid shifts of perhaps 5 K every 2500 or so years (Dansgaard *et al.* 1984a). These rapid changes in oxygen isotope values track similar changes in other chemical species measured in the Greenland ice cores: cosmogenically produced radionuclides, such as ^{10}Be, which are sensitive to changes in past precipitation rates (Oeschger *et al.* 1984); major chemical components such as sulfates, that measure marine biological productivity (Delmas and Legrand 1989); and dust and acidity values, thought to measure continental land cover and storminess (Hammer *et al.* 1985). Together, these chemical species sing a chorus of drastic change in the Arctic environment. The magnitude of these changes and the causes of these Dansgaard–Oeschger oscillations are as yet unknown.

Much study has been directed toward an event at the end of the last glaciation that appears in the ice core records to be similar to the Dansgaard–Oeschger oscillations. Beginning 12 000 to 11 000 yr B.P. (before present), this Younger Dryas event was a brief, abrupt, intense return to glacial conditions during a time of general deglaciation. During the hundreds of years the Younger Dryas lasted, the Scandinavian ice sheet halted its retreat and in some places began to re-advance (Mangerud 1980), polar plankton species replaced warmer water species in the North Atlantic (Ruddiman 1987), and herbs and heath replaced birch and pine forest in the Netherlands and Great Britain (Watts 1980). At the Gerzensee, Switzerland, pollen sediment and ^{14}C values recorded a marked cooling and change in vegetation (Oeschger *et al.* 1984). In

Greenland, the ice cores registered a roughly 7 K surface cooling, a halving of precipitation, and a several-fold increase in dust content (Dansgaard *et al.* 1989). Then, as recorded by the same ice cores, the Younger Dryas event abruptly ended. In a matter of 20 to 50 years, the climate returned to its prior condition and continued its general warming toward the conditions of the present day (Dansgaard *et al.* 1989).

1.1 A Theory for the Younger Dryas

Curiously, the effects of the Younger Dryas event mainly appear in records taken in and around the North Atlantic Ocean (Fig. 1.1). Pollen records from most of North America show no signs of a Younger Dryas cooling, while dust and oxygen isotope records from Antarctica show either a muted change in climate or no change at all (Broecker and Denton 1989). Pursuing ideas raised by Stommel (1961) and Rooth

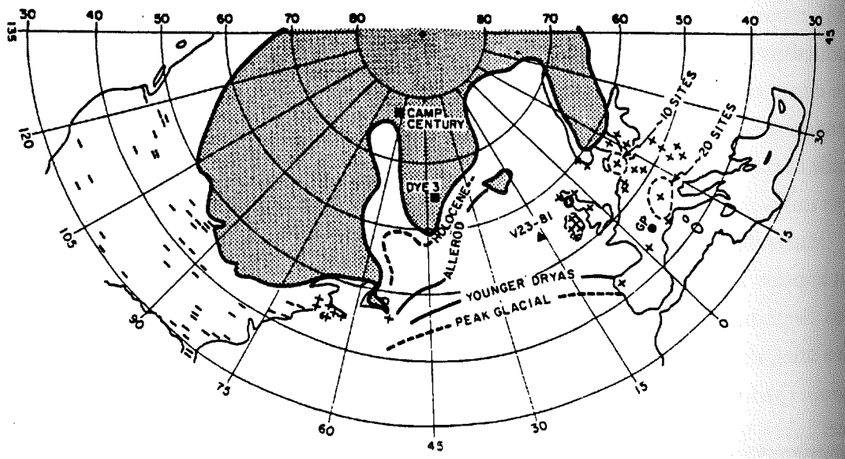

Fig. 1.1 *The location of sites recording the last deglaciation. The deep ocean cores between the lines marked Younger Dryas and Allerød, the two Greenland ice cores marked by squares, and the sites with plus signs, all show the Younger Dryas event. The sites with minus signs do not. The shaded area was covered by ice at the time of the Younger Dryas. From Broecker* et al. *(1985).*

(1982), this has led Broecker *et al.* (1985; 1988; 1990) to hypothesis that the Younger Dryas event was a result of a profound change in the North Atlantic ocean circulation.

1.11 Today's Ocean Circulation

The present day, large-scale circulation in the Atlantic ocean is a product of latitudinal heating and evaporation. In the tropics, ocean water experiences strong heating making it warmer and lighter. In the Arctic, ocean water undergoes strong cooling making it colder and denser. This establishes a thermohaline-driven circulation in which water warms in the tropics, moves northward at about 800 m depth and slowly rises. En route, it becomes saltier through evaporation. Around Iceland, it reaches the surface and then cools, sinks, and returns as a southward flowing, deep water mass (Fig. 1.2). (Smaller surface and bottom circulations also exist in the Atlantic as well as basin-scale circulations driven by the prevailing surface wind fields (Bryan and Cox 1968). These are less important to this discussion.)

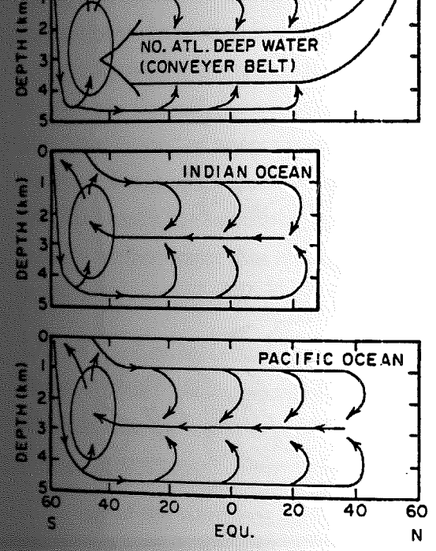

Fig. 1.2 *The major sources and flow patterns of deep water in the world oceans. Deep water is formed north of the equator only in the Atlantic Ocean. After Broecker and Denton (1989).*

The volume of water this circulation transports and the amount of heat it releases to the atmosphere are tremendous. The average flux of the southward flowing, North Atlantic Deep Water is around 20 million cubic meters per second (20 Sverdrups) while the yearly heat flux released to the atmosphere from the 8 K difference between Arctic and tropical North Atlantic waters amounts to 5 x 10^{21} calories. For perspective, these are about 20 times the combined flow of all the world's rivers and equal to 25% of the yearly solar radiation absorbed by the Atlantic ocean and atmosphere north of 35° latitude. During the Northern winter, this heat re-

leased by the ocean rivals the contribution by the sun. Were it not for this extra heat, Europe would suffer severe cold (Broecker and Denton 1989).

Of the world's oceans, the Atlantic is unique in having a pronounced return current at deep levels. In contrast, the Northern Pacific also forms large amounts of cold surface water, but none of it reaches such great depths or flows as such a great current (Fig. 1.2). It is generally agreed that this difference arises from the higher salinity found in the Northern Atlantic (Broecker *et al.* 1985). The Northern Pacific, being insufficiently saline, can not form water dense enough at the surface to sink beyond intermediate depths before matching its density and so stopping. The warmer temperatures and thus greater evaporation found in the North Atlantic compared to the North Pacific is thought to produce the higher salinity of the Atlantic Ocean (Broecker *et al.* 1985). The water evaporated from the warmer Atlantic is transported through the atmosphere and condensed onto the colder Pacific, making the Atlantic more saline and the Pacific less so. This distillation leaving excess salt in the Atlantic, is compensated by a large scale transport of salt into the Pacific by the outflow of the North Atlantic Deep Water (Fig 1.3).

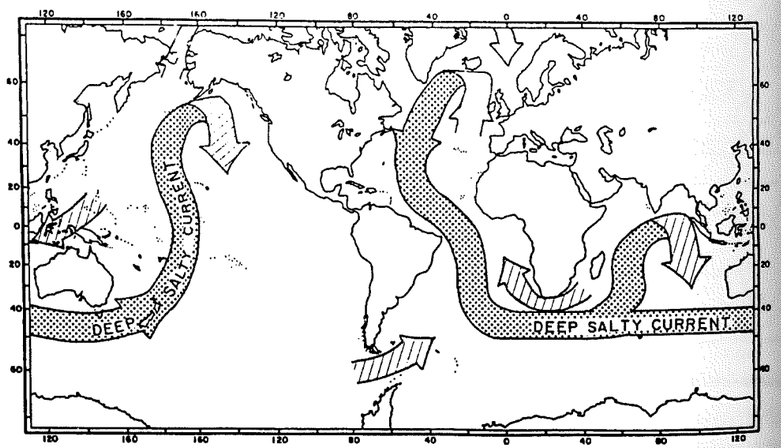

Fig. 1.3 *The large scale salt transport system that compensates for the distillation of water from the Atlantic Ocean and condensation into the Pacific Ocean. From Broecker and Denton (1989).*

1.12 The Ice Age Ocean Circulation

A similar temperature-driven transfer of water vapor is thought to occur above the North Atlantic Ocean itself, with water being distilled in the warm tropics, transported through the atmosphere, and condensed in the cold Arctic. This transfer, however, decreases the salinity of arctic waters and thus would tend to weaken the formation of a strong, deep water return current. This transfer of water vapor is not unopposed as its source water is also brought north by the upper ocean circulation. Were this circulation shut down, however, this atmospheric transport of water vapor would tend to create a layer of low salinity water at the surface of the northern-most Atlantic. Such a layer would disrupt deep water formation as in the Pacific, shut down the strong North Atlantic Deep Current, and, in turn, would reinforce the original shut down of the upper ocean circulation.

The North Atlantic ocean would greatly reduce its warming of the North Atlantic basin were its circulation shut down. The lands around it would sharply cool. Such a change would lead to ice age-like conditions, and indeed, Broecker *et al.* propose that a shut down circulation is the Atlantic's ice age condition however, only episodically. According to their theory, such a condition is unstable. With the general circulation in the Atlantic shut off, the export of salt by the North Atlantic deep current would cease. The "distillation" of water vapor from the Atlantic and "condensation" to the Pacific, however, would continue so that the salinity of the North Atlantic would start to slowly rise. Eventually, the salinity of the North Atlantic would again reach high enough levels to form surface water that could sink to great depths. This would revive the North Atlantic deep current and restore the Atlantic Ocean's general circulation.

1.13 A Smoking Gun

The story so far has suggested the Atlantic Ocean exists in one of two conditions. First, a "circulation on" condition like the present day in which:

- warm water rises to the surface in the North Atlantic, maintaining the salinity of the northern surface waters, and warming the northern basin and surrounding lands;
- high salinity water cools in the North Atlantic and sinks to great depths;
- a vigorous return circulation forms at deep levels to carry excess salt to the Pacific.

Second, an ice age, "circulation off" condition in which:

- no warm water flows to the North Atlantic, cooling the basin and surrounding lands and exacerbating the salinity of northern Waters;
- insufficiently saline water cools in the North Atlantic but sinks only to intermediate depths;
- a deep return current fails to form to carry excess salt to the Pacific.

According to the story, this last situation causes salt to accumulate in the North Atlantic so that if the ocean is in a "circulation off" condition, eventually it turns back "on." What is missing from the story so far is how the North Atlantic could flip the other way: go from being more saline to less, and from having a strong circulation to having none. Since the story implies that a strong circulation is self-reinforcing, there needs to be some trigger to flip the Atlantic out of this stable state and so complete the circulation-on / circulation-off cycle.

Broecker and Denton (1989) suggest that such circulation and climate cycles occurred repeatedly during the ice age and the transition to the present inter-glacial. They propose the Dansgaard–Oeschger $\delta^{18}0$ oscillations as one example recording the Atlantic Ocean circulation cycling on and off. The trigger, they suggest, was a succession of fresh water pulses into the North Atlantic that repeatedly diluted the surface water to North Pacific salinity levels, killed off the North Atlantic deep current, and shut down the Atlantic Ocean's large scale circulation. The Younger Dryas event they see as a later example. It appears in the records to be similar to the Dansgaard–Oeschger oscillations and its onset coincides with a particular, well recorded, influx of meltwater into the North Atlantic. As such it provides a test of these ideas, or as Broecker and Denton put it, "... a smoking gun which links ocean circulation to fresh water transport."

1.14 Glacial Lake Agassiz and the Younger Dryas

At the end of the last glaciation, a large lake developed at the southern edge of the Laurentide ice sheet, Lake Agassiz (Fig 1.4). It formed from melt water trapped between the retreating ice sheet and the tilted, newly exposed land, still rebounding from the great mass of ice that sat upon it during the height of the glaciation at 18 000 yr B.P. Around 12 000 yr B.P., much of this water overflowed into the Mississippi River in a large flood and left its imprint in the chemical isotope values of sedimentary carbonates in the Gulf of Mexico and the alluvial fans on the Mississippi River (Emiliani *et al.*

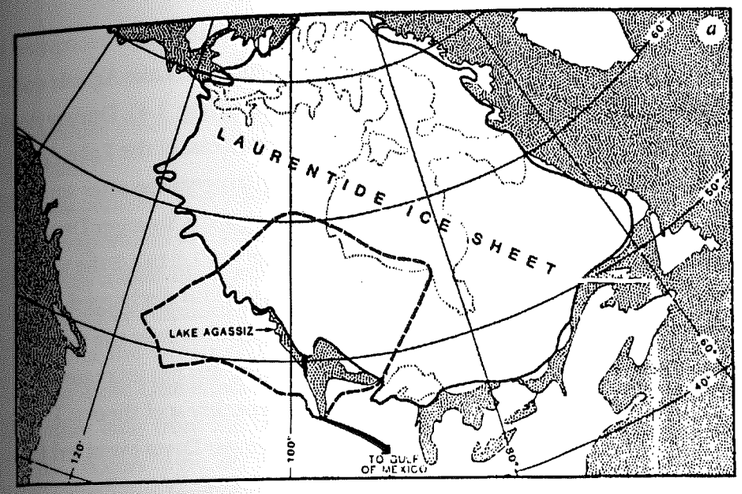

Fig. 1.4 The Laurentide Ice Sheet and routing of overflow from Lake Agassiz basin (dashed outline) to the Gulf of Mexico. After Broecker et al. *(1989).*

1978; Leventer *et al.* 1982; Broecker *et al.* 1988). However, between roughly 11 000 and 10 000 yr B.P. (the time of the Younger Dryas), the ice had sufficiently retreated to allow a complicated series of diversions to shunt water down the St. Lawrence and into the North Atlantic (Teller 1985). During this period, little meltwater reached the Mississippi. Around 10 000 yr B.P., the Laurentide ice sheet re-advanced into Lake Superior, and this outflow was again sent down the Mississippi.

Broecker *et al.* (1985, 1988) originally proposed that this diversion of Lake Agassiz water into the St. Lawrence directly forced the Younger Dryas event: The start of the diversion, they proposed, sufficiently increased the flux of fresh water into the North Atlantic to reduce its salinity, to shut off deep water formation and to cause the Younger Dryas event as outlined above. The diversion of water down the St. Lawrence continued during the Younger Dryas to prolong the event. Finally, the redirection of meltwater back to the Mississippi at the end of the Younger Dryas sufficiently decreased the flux of fresh water into the North Atlantic to allow its salinity to rise and to end the event. Interpreted this way, the Lake Agassiz meltwater disappeared from the Mississippi causing the Younger Dryas event and reappeared afterward allowing the event to end.

With this focus on the fate of Lake Agassiz, it is important to recognize Lake Agassiz's limited meltwater contribution to the North Atlantic. Lake Agassiz collected melt water from only a fraction of the Laurentide ice sheet (Fig. 1.4). During deglaciation, the North Atlantic's principle fresh water supply was east of the Lake Agassiz basin. Fairbanks (1989) discovered a problem with this interpretation after studying the sea level rises recorded by coral reefs off Barbados. During the Younger Dryas period, the rate of meltwater discharge by the world's ice sheets was 1/3 to 1/5 the volume just prior to and just after the event. As Lake Agassiz collected and discharged only a fraction of the Laurentide ice sheet's meltwater, this suggests that over the period of the Younger Dryas, the meltwater flux into the North Atlantic was not increased but likely reduced, just the opposite condition required by the Broecker *et al.* theory. The lack of a large flux of fresh water to cause and maintain the Younger Dryas event led Broecker *et al.* to reexamine their diversion theory in the light of Fairbanks's meltwater record. It also led Fairbanks to propose a different explanation for the Younger Dryas, an explanation intimately tied to the Barbados meltwater record and the oxygen isotope records of the last deglaciation.

1.2 Other Theories for the Younger Dryas

1.21 Ice Sheets and Delta O-18

Natural water is composed of normal $H_2{}^{16}O$ and several isotopes. The most important of these are the two heavy species, $HD^{16}O$ and $H_2{}^{18}O$ (where D ≡ deuterium). The vapor pressures of the two heavy species are slightly less and so they evaporate slightly less readily and condense slightly more readily than normal $H_2{}^{16}O$. As a result, if a body of water partially evaporates, the water left behind tends to be slightly heavier. If the vapor from the same body of water progressively condenses out, the precipitation formed at each stage is lighter and becomes more so.

The magnitude of these fractionations is fairly small. The ratio of the concentrations of the heavy and normal isotopes measured in a sample, R_s, is measured in terms of its deviation from the ratio measured in "standard mean ocean water," R_o, and then expressed as a "delta" value by the formula:

$$\delta = 1000\frac{R_s - R_o}{R_o} \qquad (1.1)$$

Minimum values observed in nature are about -60‰ for $\delta^{18}O$ and -500‰ for δD (Paterson 1981).

Such fractionation processes are important over a glacial cycle. During glaciation, there is net evaporation of water from the ocean and deposition on land. As glaciation progresses, this makes the ocean isotopically heavier and the ice sheets isotopically lighter. Water vapor evaporated from the ocean is lifted and cooled as it comes inland. As it travels over the surface of the ice sheets, the vapor progressively cools and condenses out as snow. One effect is to make an ice sheet increasingly light, isotopically, moving further away from the ocean. The other is that as an ice sheet thickens, the condensation occurs at greater heights and thus lower temperatures.

These "source distance" and "elevation" effects make the ice formed in an ice sheet isotopically light. Typical $\delta^{18}O$ values for Greenland ice run -20 to -40‰ compared to 0‰ for standard ocean water. Lower precipitating cloud temperatures are believed to make the ice formed during an ice age isotopically lighter compared to the ice formed today.

Dansgaard *et al.* (1973) found that the dominant factor in determining the $\delta^{18}O$ values in the Greenland ice sheet is the difference between the condensation temperature in the precipitating cloud and the temperature at the first stage of the condensation process. For snow recently deposited at different sites in central Greenland, Dansgaard *et al.* found a decrease in $\delta^{18}O$ with mean annual surface temperature of about 0.62‰ per °C. From this, they concluded that a site's mean annual surface temperature is closely related to the temperature of its precipitating clouds and that the $\delta^{18}O$ value is most strongly determined by the clouds' condensation temperatures. For recent times, this implies that the temperature at the start of condensation is essentially the same for different sites in Greenland.

Sea-surface temperatures at mid to high latitudes are more stable than air temperatures at high latitudes; relatively speaking, the temperature at the start of condensation should also be similar during an ice age. Air temperatures during an ice age are markedly colder. This should increase the difference between the starting and precipitating condensation temperature and make the ice formed during an ice age especially light compared to today.

The $\delta^{18}O$ values measured in the Dye 3 ice core ice are roughly 8‰ lower in ice deposited near the end of the last ice age than in snow deposited today. Temperatures at that time are thought to have been 10–15 K cooler (CLIMAP 1981; Dahl-Jensen and Johnsen 1986). Assuming the present day relation of 0.62‰ per °C, an 8‰ change translates to a 13 K cooling in agreement with these temperature estimates.

1.22 Melt Water and the Delta O-18 Record

During deglaciation, the light isotopic species concentrated in the ice sheets are restored to the oceans through melting and evaporation. As the Younger Dryas event occurred in the midst of the last deglaciation, it is instructive to compare the $\delta^{18}O$ records of the last deglaciation as seen in an ice sheet (the Dye 3 ice core) against the

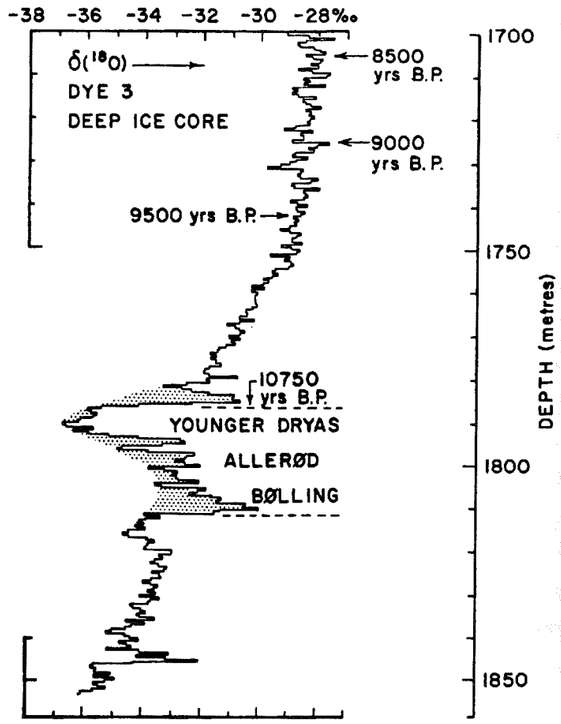

Fig. 1.5 The oxygen isotope record at Dye 3, Greenland over the last deglaciation. After Paterson and Hammer (1987).

record as seen in a North Atlantic ocean core (core SU81-18 off Portugal). Both records (Fig. 1.5 and 1.6) show complementary trends in $\delta^{18}O$ values, the ice core record becoming less negative and the deep ocean record becoming less positive, in accord with an isotopically "heavy" ocean becoming lighter as water from very light glacial ice returns to the ocean.

Superimposed on the complementary upward and downward trends, is a marked, brief reversal in the $\delta^{18}O$ values, centered around the time of the Younger Dryas, in the ice core record, and around the 10 200 radiocarbon yr B.P., in the ocean core record. As was mentioned previously, the general consensus is that this was a period of marked cooling. The reversals in both these oxygen isotope records can and have been explained by the effects of about 7 K of cooling (Hammer *et al.* 1986; Boyle and Keigwin 1987; Dansgaard *et al.* 1989; Keigwin and Jones 1989) However, glacial meltwater changes may provide an additional or equally good explanation.

According to the Barbados sea level record (Fairbanks 1989), the last deglaciation was punctuated by two large glacial meltwater pulses centered around 12 000 and 9 400 radiocarbon yr B.P. with a lull in between spanning the Younger Dryas (Fig 1.7). At these same times, the ocean core SU81-18, off Portugal, shows two rapid decreases in $\delta^{18}O$ values and a modest increase (Fig 1.6). At similar times, (in Figure 1.5, the "Younger Dryas", "pre-Bølling," and "Allerød/Bølling"), there are decreases and an increase in the Dye 3 isotope record. It is not hard to imagine that rapid discharges of glacial meltwater with $\delta^{18}O$ values of -30 to -40‰ left some imprint on the ice and ocean core records. The similarities in these three records have led Fairbanks (1989) to suggest a different explanation for the

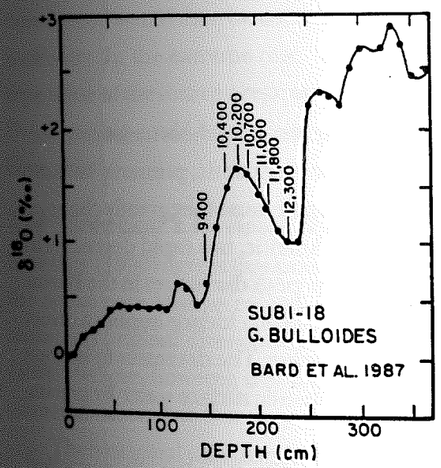

Fig. 1.6 The oxygen isotope record for planktonic species G. bulloides over the last deglaciation from core SU81-18 off Portugal. The dates shown are radiocarbon (^{14}C) dates. The corresponding calendar dates are roughly 1000 years older. From Broecker (1990).

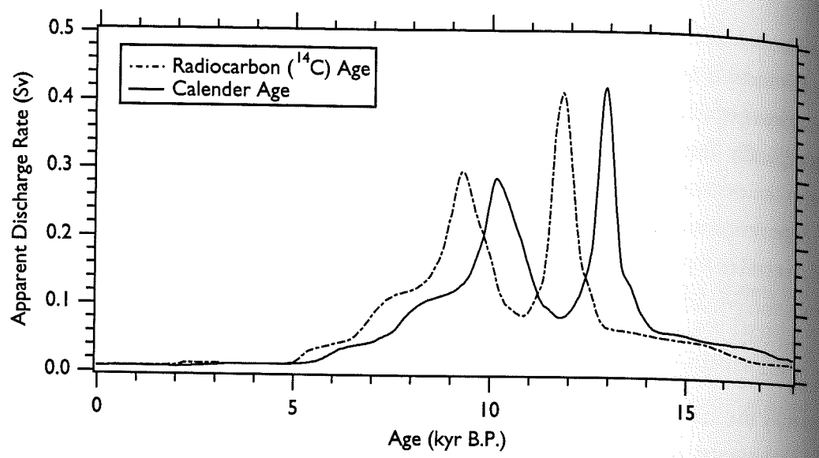

Fig. 1.7 *The rate of glacial meltwater discharge calculated from the Barbados sea level curve. The discharge is shown plotted against both radiocarbon (^{14}C) and calender years. After Fairbanks (1989).*

Younger Dryas tied directly to glacial meltwater.

1.23 Fairbanks's Theory for the Younger Dryas

Fairbanks's thesis is that over the last deglaciation, the influx of ice sheet meltwater controlled the oxygen isotope records in and around the North Atlantic, primarily because the influxes made the ocean isotopically light, rather than because they greatly changed its salinity, temperature, and circulation. In the North Atlantic, two rapid decreases in the ocean core isotope values (Fig. 1.6) coincide with the peak discharges in the Barbados sea level record (Figs. 1.7). Fairbanks believes that the coincidence implies a direct communication of isotopic "lightness" from one to the other. The decreases in isotope values, he believes, record two invasions of the North Atlantic surface water by gravitationally and isotopically light water from the ice sheets.

Secondarily, according to his theory, the influx of ice sheet meltwater controlled the North Atlantic ocean isotope record, because the freshwater influxes made the ocean surface water less saline. This is revealed by the rise in the oxygen isotope value during the Younger Dryas, which marked a hiatus between these floods. Before and after, the influx of fresh meltwater depressed the salinity of the surface waters of the

North Atlantic. Analogous to the present day Northern Pacific, the lower salinities resulted in a thinner surface mixed layer with lower thermal inertia. The results of a global climate model suggest that this led to warmer summer surface temperatures (Schneider *et al.* 1987) over the North Atlantic Basin. During the Younger Dryas, the lack of meltwater allowed the salinity of the surface waters to increase. This temporarily restored a deeper mixed layer and returned the summer North Atlantic and surrounding lands to cooler glacial conditions.

The results from the global climate model suggest that this warming and cooling would be most pronounced over Western Europe, roughly 4 to 8 K, and less so over central Greenland, roughly 2 K at Dye 3. This is at odds with the common belief that the Younger Dryas cooling in Greenland was nearly as strong as in Western Europe. A limited radiocarbon dating of portions of the Dye 3 ice core suggests that "Younger Dryas" and "pre-Bølling" minima of the Dye 3 oxygen isotope record (Figure 1.5) might, in fact, coincide with the meltwater peaks of the last deglaciation. Suppose, as Fairbanks asks, that this meltwater invaded the source water for central Greenland's precipitation. The presumed 7 K cooling that many researchers see in the Dye 3 ice core record would then be tainted by secondary distillation of isotopically light surface meltwater. In the extreme case, this "cooling" might all be due to changes in the isotope value of the source ocean water. If the global climate model is correct, the Younger Dryas cooling could have occurred over Western Europe but might not have reached Greenland.

1.24 Broecker's Revised Theory for the Younger Dryas

Broecker (1990) agrees that isotopic meltwater effects must have left some imprint on the ocean core isotope record. He admits that Fairbanks's glacial meltwater history makes his original diversion theory untenable. Broecker (1990) and Broecker *et al.* (1990) believe, however, that the history suggests not that they discard the meltwater diversion theory but that they augment it.

Their original idea that the diversion of meltwater from Lake Agassiz to the North Atlantic was the sole cause of the Younger Dryas was too simple. Broecker (1990) and Broecker *et al.* (1990) continue to believe that the Younger Dryas cooling resulted from an oscillation in the Atlantic Ocean circulation as described earlier. Instead, they see the spike of fresh water during the Younger Dryas as triggering a transition in a circulation oscillation already in progress. Broecker (1990) suggests that high rates of melt-

water flux prior to the Younger Dryas initiated a single oscillation of the circulation by lowering the salinity of the North Atlantic and weakening the North Atlantic deep current. The flux of meltwater from Lake Agassiz then pushed the North Atlantic over the brink. Broecker *et al.* (1990) suggest that such oscillations occur naturally in the Atlantic during glacial times without any need for external fresh water forcing. In this interpretation, the spike of fresh water during the Younger Dryas only fixed the time of the last oscillation.

1.3 Distinguishing the Theories for the Younger Dryas

1.31 A Difference in Meltwater

The theories of Broecker and Fairbanks both call on meltwater floods to either pace or directly cause changes in the North Atlantic ocean circulation. Both then call on these circulation changes to cause the climatic changes surrounding the Younger Dryas. In Broecker's theory, the meltwater flood during the Allerød warming greatly weakened the North Atlantic ocean circulation; the diversion of meltwater from Lake Agassiz into the North Atlantic during the Younger Dryas then shut it down completely to cause the Younger Dryas cooling. In Fairbanks's theory, the meltwater floods at 12 000 and 9400 radiocarbon yr B.P. decreased the depth of the North Atlantic's mixing layer to cause the Allerød and post Younger Dryas warmings; the meltwater hiatus in between allowed the depth of the mixing layer to increase, to cause the Younger Dryas cooling.

Both theories call on floods of fresh water to decrease the salinity of the upper waters of the North Atlantic and reduce vertical mixing, but to different degrees. In Broecker's theory, the floods greatly decrease the salinity and eventually cause all vertical transport in the North Atlantic to cease (i.e. they shut down the North Atlantic deep water current). In Fairbanks's theory, the floods decrease the salinity and reduce the depth of vertical mixing, but they still allow the North Atlantic deep water current to operate.

The two theories differ completely in the degree to which meltwater isotopic effects explain the features in the North Atlantic and Greenland oxygen isotope records. Fairbanks supposes that glacial meltwater remains isotopically light as it mixes with the ocean and explains most of the variation in the records. Broecker supposes that it does not, or even if it does, that its lightness has little effect. This difference is most apparent

in their explanations of the Dye 3 $\delta^{18}O$ record (Fig. 1.5). Fairbanks attributes much of the "cooling" during the portions marked pre-"Bølling" and "Younger Dryas" to isotopically light meltwater entering the record. Broecker does not allow this possibility and maintains that the cooling is real.

1.32 A Difference in Temperature

This difference is worth stating more explicitly. The temperature contrast between the ice age and today estimated from the Dye 3 $\delta^{18}O$ record is thought to be roughly 13 K (Paterson and Hammer 1987). The Younger Dryas is thought to have started around 11 500 yr B.P., to have abruptly ended at 10 700±150 yr B.P., and to have represented a cooling of roughly 7 K. If the Dye 3 $\delta^{18}O$ record is a faithful record of the temperature, as Broecker believes, ignoring more recent changes, an idealized temperature record for the deglaciation in agreement with Broecker's theory might look like the left pane of Figure 1.8. Call this Scenario B. If the rapid changes in the record are purely meltwater effects as Fairbanks suggests, an idealized temperature record in agreement with a most extreme interpretation of Fairbanks's theory might look like the center pane of Figure 1.8. Call this Scenario F1.

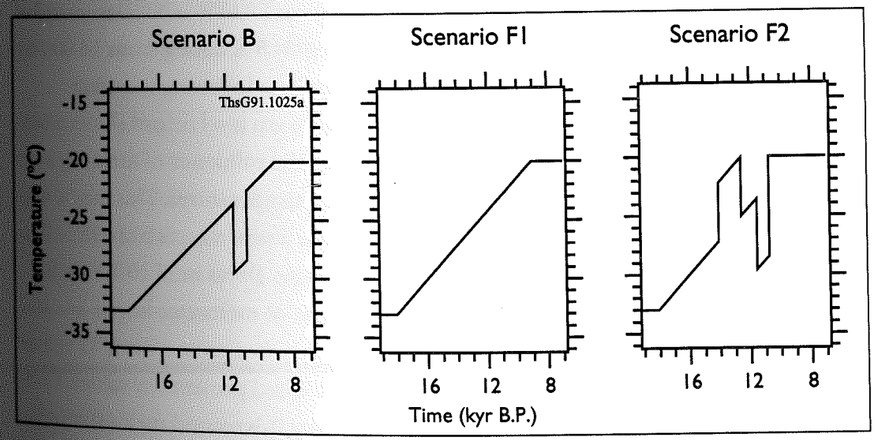

Fig. 1.8 Three idealized temperature histories suggested by the Dye 3 oxygen isotope record: Scenario B, consistent with Broecker's theory, and Scenarios F1 and F2, consistent with Fairbanks's theory.

The Barbados sea level record centers the two main glacial meltwater pulses of the last deglaciation at 12 000 and 9,400 radiocarbon yr B.P. Fairbanks has translated these as 13 000 and 10 000 calendar yr B.P. (Fig. 1.7). Fairbanks matches the two minima in the Dye 3 $\delta^{18}O$ record to the peak discharges at these times. One objection to Fairbanks's theory is that these two minima have been dated as belonging to the Younger Dryas and pre-Bølling periods which occur significantly earlier (Dansgaard *et al.* 1989). If Fairbanks has correctly matched the events in the two records, this implies that either the Dye 3 or Barbados records have been incorrectly dated. On the other hand, both records could be correctly dated and Fairbanks's correlation could be wrong. Assuming the correlation is wrong but that the features in the Dye 3 core largely reflect the glacial meltwater rate, a third scenario suggests itself.

At the start of the Bølling warm period, perhaps 14 000 yr B.P., the $\delta^{18}O$ value in the Dye 3 record increased by roughly 3‰. It remained at that value for perhaps 500 years, fell back by an equal amount by the start of the Allerød, and then decreased slightly with occasional downward spikes until the start of the Younger Dryas. (Fig 1.5). According to the Barbados sea level record, the first glacial meltwater pulse began 13 500 yr B.P. and continued for roughly 1000 years. Suppose that the rise in sea level at the start of the Allerød represents warming, that this warming continued, and that a meltwater pulse then entered the Dye 3 record so as to just cancel the warming that would have appeared in $\delta^{18}O$ values. Using the conversion of 0.62‰/°C (Dansgaard *et al.* 1973), this might suggest a warming period of roughly 5 K lasting from 14 000 to 12 500 yr B.P. This is not a unreasonable history for melting following warming.

From roughly 12 500 to 10 500 yr B.P., the Barbados sea level record shows a hiatus in glacial melting. Suppose that this greatly reduced the influence of meltwater on the Dye 3 $\delta^{18}O$ record so that again it faithfully recorded temperatures. This might suggest a drop in temperature of 5 K at 12 500 yr B.P., steady temperatures from 12 500 to 11 500 yr B.P., and then 7 K of cooling during the Younger Dryas until 10 700 yr B.P.

According to the Barbados record, a second pulse of meltwater began around 10 500 yr B.P. and lasted for roughly 1000 years. Over the same period the $\delta^{18}O$ values in the Dye 3 record increased by roughly 3–4‰ and reached present day values. Continuing in the spirit of the Fairbanks theory, suppose that this second meltwater pulse has masked warming and that the rise in $\delta^{18}O$ values over this period reflects its decaying influence on the $\delta^{18}O$ record. Without a great leap of faith this might imply a 5 K

change to present day temperatures at 10 500 yr B.P.. A final idealized temperature history in agreement with this reinterpretation of Fairbanks's theory might look like the right pane of Figure 1.8. Call this Scenario F2.

1.33 How to Choose?

Both Broecker and Fairbanks advance plausible explanations for the climatic changes that occurred during the Younger Dryas. The true explanation for this event may incorporate elements from both or perhaps neither. The $\delta^{18}O$ values recorded at Dye 3 could be a combination of effects from both theories. These scenarios, B, F1, and F2, perhaps represent end members consistent, respectively, with Broecker's and Fairbanks's explanations. Here are two possible theories for the cause of the Younger Dryas yielding three scenarios. Which is more plausible and how to choose?

CHAPTER TWO

A Heat Flow Model

THE ISOTOPE RECORD from Dye 3 presents a most detailed and sensitive history of the last deglaciation. Yet, for the present discussion, this is a great disadvantage. The problem is that it is sensitive to too many things. Among other things and in particular, the record combines the effects of temperature changes and glacial meltwater influxes. To choose among the theories of Broecker and Fairbanks, requires an independent record of one or the other.

It has long been recognized that the temperature measured in an ice sheet varies with depth and that these variations should tell something about the ice sheet's past climate (Koch and Wegener 1930; Sverdrup1935). Many holes have been bored in the Arctic and Antarctic ice sheets. Over the years, a number of researchers have measured the temperatures in these boreholes and then used geophysical heat flow models to estimate past temperatures, accumulation rates, and flow laws (Weertman 1968; Paterson and Clarke 1978; Budd and Young 1983; Bolzan 1985; Ritz 1989; Alley and Koci 1990).

Johnsen (1977) examined the temperatures from two shallow holes drilled in Central Greenland, applied a simple model of the temperature in firn, and was able to show that the temperatures in the boreholes were consistent with proxy records of the past surface temperature. At Crête, Johnsen showed that the temperatures measured in the top 50 m of the firn agreed with the variation of $\delta^{18}O$ with depth. At Dye 3, he showed that the temperatures in the top 90 m were consistent with the last 80–100 years of temperature records from the east and west coasts of Greenland.

The temperatures over the 2037 m of the Dye 3 borehole have been measured several times (Gundestrup and Hansen 1984; Hansen and Gundestrup 1988) during and following drilling. Using the temperatures taken from earlier loggings and a temperature model similar to Johnsen's, Dahl-Jensen and Johnsen (1986) were able to estimate the temperature difference between the ice age and today and to reconstruct many of the known temperature changes of the last few millennia.

We could say more about the theories of Broecker and Fairbanks if we could separate the temperature and meltwater effects in the Dye 3 isotope record. Could these same borehole temperature measurements tell something about the temperature history during the Younger Dryas?

2.1 The Geophysical Setting of Dye 3

To answer that question first requires an accurate model of the heat flow at Dye 3. Such a model will need to consider the ice flow and other geophysical conditions at Dye 3.

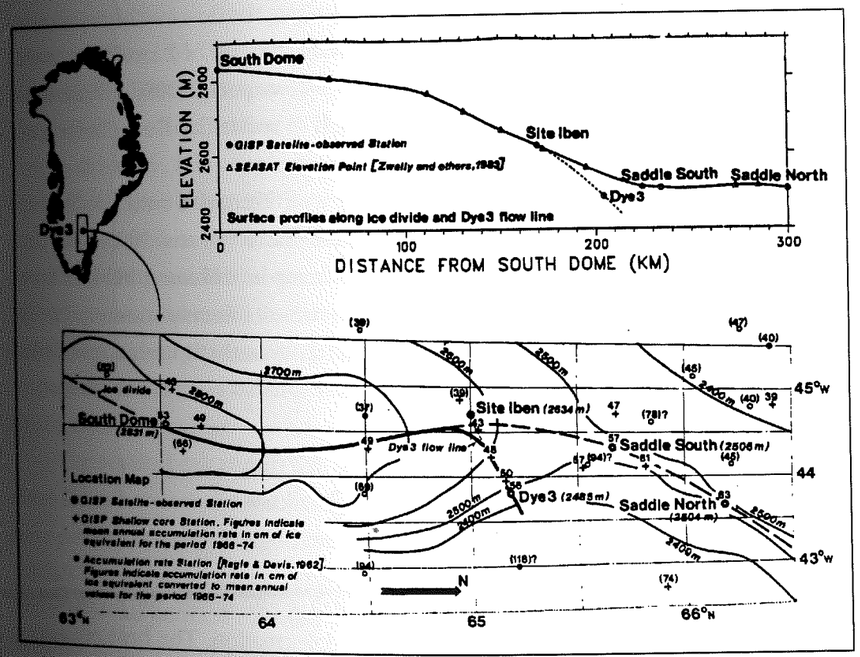

Fig. 2.1 Location map, surface elevation profile, and flow-line between South Dome and Dye 3. The dotted line of the elevation profile corresponds to the flow-line from Site Iben to Dye 3. From Reeh et al. *(1985).*

Figure 2.1 shows the Greenland Ice Sheet and the location of the Dye 3 borehole (65° 11' N, 43° 49' W). The ice sheet has an area of approximately 1.67 x 10^6 km^2 and a volume of 2.83 x 10^6 km^3. It has two domes of 2830 and 3210 m elevation, one in the south and one near the center, joined by a north–south ridge. Dye 3 is located on the eastern flank of the north–south ridge approximately 40 km from the divide. The estimated flow-line through Dye 3 (the bold line in the bottom pane of Fig 2.1) originates at the South Dome, roughly 200 km south, follows the ridge line until it passes by Site Iben, and then veers east to continue through Dye 3. The ice sheet thickness at Dye 3 is 2033 m (Gundestrup and Hansen 1984). Flow modelling indicates that most of the ice in the Dye 3 core (the upper 1700 m) was deposited over the last 8000 years in the area between the drill site and the vicinity of Site Iben (Reeh *et al.* 1985).

Between South Dome and South Iben, the average ice sheet surface elevation drops approximately 200 m (solid line, top pane) and between South Iben and Dye 3, another 150 m (dashed line, top pane). The bedrock along the flow-line is very mountainous with elevation changes exceeding 400 m over a distance of 2 km (Overgaard and Gundestrup 1985). Ice thicknesses along the flow-line average 2000 m and show comparable changes. This is a difficult area in which to model ice flow (Reeh *et al.* 1985).

The horizontal surface velocity at Dye 3 is 13.2 m/a (Overgaard and Gundestrup 1985). The annual precipitation is 0.55 m, water equivalent (Reeh *et al.* 1985), and the mean annual surface temperature is -20.1° C (Gundestrup and Hansen 1984). There is always some surface melting during the summer; however, this only occasionally disturbs the stratigraphy of the core and not so much as to make it un-interpretable. (Dansgaard *et al.* 1984b 1985).

2.2 Heat Flow Models for Dye 3

2.21 Heat Transfer Equations

Because Dye 3 is located some distance from the north–south divide, the ice at Dye 3 has experienced significant horizontal and vertical deformation. The heat equation for a deforming medium can be written in terms of temperature, T, time, t, and Cartesian coordinates, x_m, as

$$\rho c\left[\frac{\partial T}{\partial t}+v_m\frac{\partial T}{\partial x_m}\right]=f+\frac{\partial K}{\partial x_m}\frac{\partial T}{\partial x_m}+K\nabla^2 T \qquad (2.1)$$

where ρ, c, and K are the material density, heat capacity, and heat conductivity, v_m, the velocity vector, and f, the rate of internal heat production per unit volume (Paterson and Clarke 1978). For an ice mass, f is the sum of strain heating and latent heating contributions

$$f=\sigma_{ij}d_{ij}+w \qquad (2.2)$$

where σ_{ij} and d_{ij} are the stress and strain rate tensors, and w is the rate of release of heat per unit volume due to freezing of meltwater (Paterson and Clarke 1978).

For an ice sheet, equation (2.1) couples to a set of momentum-conservation equations through the velocity terms, v_m, and the variation of ice rheology with temperature (Hutter 1983, c. 3). The solution of the full set of time-dependent equations is quite involved. For lack of adequate boundary conditions, such a solution has not been attempted for the flow leading to Dye 3.

In this work, I de-couple the coupled heat and mass flow equations. Previous ice flow models have solved the momentum conservation equations at Dye 3 assuming steady-state, present day conditions (chiefly the present day geometry, accumulation rates, and temperatures). I use the results from these models to establish a modern velocity pattern. I assume that the ice sheet geometry around Dye 3 has not changed but allow the precipitation rate (mass balance) to vary over time. I then scale the velocity pattern to the mass balance and apply this velocity field to the (time-dependent) heat transfer equations.

The results I can obtain this way are most realistic for recent times. For more ancient times, however, the results are increasingly limited by my assumption that the flow field pattern has not changed over time. The Greenland ice sheet was perhaps 150 m thicker along the north–south divide during the last ice age (Reeh 1984). The precipitation rate was perhaps 1/3 today's value (Dansgaard *et al.* 1989). These changes would alter the stresses controlling the ice flow pattern. The net effect on the velocity pattern and, in turn, the temperature field is complicated and unknown.

2.22 Thermal Media and Internal Boundaries

Near Surface Firn Snow that precipitates onto an ice sheet transforms over depth, through settling and sintering, to firn and finally to ice. At Dye 3, the firn / ice transition is reached at 65–70 m depth (Paterson 1981, c. 1). Above this depth, the density, thermal conductivity, and heat capacity of the snow vary. These variations do have a significant effect on recent temperature changes within the topmost parts of the Greenland ice sheet (cf. Johnsen 1977; Paterson and Clarke 1978).

With a simple scale analysis, I can determine the effects of these variations on older temperature changes at greater depths. If I consider only the vertical heat flow at Dye 3 and neglect what are likely lesser effects (e.g. strain heating), I can write (2.1) as

$$\frac{\partial \theta}{\partial t} = \frac{\partial}{\partial z}\kappa\frac{\partial \theta}{\partial z} - v_z\frac{\partial \theta}{\partial z} \tag{2.3}$$

where θ is the temperature, κ is the diffusivity of snow, and v_z is the vertical velocity. If I define K, *V*, *L*, and Θ to be typical values for the firn diffusivity, vertical velocity, distance from the surface, and temperature change, I can list the characteristic sizes of the terms in (2.3):

$$\frac{\Theta}{L} \qquad \frac{K\Theta}{L^2} \qquad \frac{V\Theta}{L}. \tag{2.4}$$

The two right-most terms can be combined to form the *Peclet* number,

$$Pe = \frac{VL}{2K} \tag{2.5}$$

which measures the importance of advection to diffusion. A problem will have diffusion-dominated flow if the Peclet number is less than one; it will have an advection- or convection-dominated flow if the number is greater than one.

The Peclet number increases linearly with a problem's characteristic length scale. Thus, at Dye 3, I can expect that advection will become increasing important in carrying a surface temperature change to greater depths. Neglecting heat transfer by forced convection, the effective diffusivity of snow is less than ice (Yen 1981). Using a typical ice diffusivity of 36 m^2a^{-1} as an upper bound for K and the observed Dye 3 accumulation rate of 0.5 ma^{-1} for V_z, the Peclet number for propagating a surface temperature change over depth will have a value of one at a depth of roughly 150 m. A surface temperature change reaches 150 m depth in less than 300 years time. Below 150 m (or after 300 years), the Peclet number will be greater than one, indicating that the surface temperature change propagates predominantly by advection.

In the models for this study, I neglect the effects of the thermal variations in the top 65–70 m of firn and I reduce the firn to its ice equivalent. By doing so, I misrepresent the diffusion in the firn. At deeper levels, this will change the phase and amplitude of the response to surface temperature changes. In this study, I will only consider surface temperature variations of hundreds to thousands of years duration that have reached the lowest portions of the ice sheet. On those time and length scales, surface temperature changes are transmitted predominantly by advection. I expect the changes in phase and amplitude will be fairly small.

Ice and Ice Equivalent I, therefore, treat the firn and ice at Dye 3 as pure ice and I convert the firn to its ice-density equivalent. This reduces the ice thickness at the Dye 3 borehole by 24 m to an ice-equivalent thickness of 2009 m (Reeh 1989a). For a slight loss of accuracy, I reduce all vertical distances by a further 0.45%. In the models, I treat the firn and ice at the Dye 3 borehole as a single 2000 m thick layer.

Bedrock The bedrock below an ice sheet provides transient thermal storage and influences the heat flux into the base of the ice sheet (Paterson and Clark 1978, Budd and Young 1983; Ritz 1987; Waddington 1987). To account for this in the models, I place a 3000 m thick layer of bedrock below the ice sheet. At the bedrock / ice sheet interface, I impose a continuous heat flux, that is, I assume no melting. (This will prove to be a realistic assumption, cf. §2.41)

2.23 Boundary Conditions

Basal Boundary Condition Because of its great thickness and slow movement, the lower portions of the central Greenland ice sheet are warmed by the outflow of heat from the earth (Robin 1955). To include this effect in the models, I introduce a constant geothermal heat flux at the bottom of the bedrock.

Surface Boundary Condition At the ice sheet's surface, I apply a temperature forcing. I have a number of choices for this forcing.

Since I seek a temperature history for Dye 3 to compare against the Dye 3 $\delta^{18}O$ record, I might apply a temperature forcing that is most directly related to the "temperatures" recorded in the Dye 3 $\delta^{18}O$ values. As mentioned §1.21, this temperature

forcing would be the temperature of the clouds precipitating snow onto the ice sheet. In practice, this choice of forcing suffers from two difficulties.

The first difficulty is to relate the cloud temperature during storms to the ground temperature. This requires modelling the Rayleigh condensation/sublimation of snow from the cloud. This is complicated, it requires several "tuning" coefficients, and it suggests temperatures on the ground that are 4–5 K higher than in the clouds (Johnsen *et al.* 1989). If these differences were consistent from storm to storm and season to season, the effects of these differences could be removed from the analysis. However, they may not be consistent.

The second difficulty is to relate the ground temperature during storms to the mean annual temperature. During the winter, strong temperature inversions form in central Greenland. The warm air masses that bring winter snow can temporarily increase the surface temperatures by up to 20 K. Modelling suggests that during the coldest months, the ground temperature during storms rises to 15 K above the mean monthly temperature (Johnsen *et al.* 1989). Again, if this difference was consistent from storm to storm and season to season, its effects could be removed from the analysis. However, it may not be consistent.

I seek a temperature history for Dye 3 that I can compare against the coolings and warmings predicted by Broecker and Fairbanks. As an alternative, I might make the mean annual air temperature above Dye 3, the temperature forcing in the models. In practice, this choice of forcing suffers from a major complication. Surface melting during the summer injects latent heat that warms the near surface snow. In an extreme example, Paterson and Clarke (1978) modelled the temperatures in the Devon Island ice cap and found that the refreezing of surface meltwater during the summer obliterated the temperature variation they imposed at other times.

The summer melting at Dye 3 is not quite so great. Johnsen (1977) was able to relate $\delta^{18}O$ "temperatures" to mean annual temperatures. However, if I wanted to interpret the forcing as a true air temperature, I would have to estimate the extra heat flux introduced by summer melting into the top few meters of firn. I could estimate the flux from ice core melt layer thicknesses as in Paterson and Clarke. However, melt layer records for Dye 3 have not been published.

Instead, I apply a temperature at the surface of the 2000 meters of ice-equivalent and I interpret the temperature as an effective temperature forcing. This forcing is

something like the temperature measured at 10 m depth in a snow field. It represents the seasonally integrated effects of the surface temperature and surface melting. Its variation is probably related but not identical to the mean annual temperature at the surface. In spite of surface melting, it is likely that this effective temperature will be effective in detecting the warmings and coolings predicted by Broecker and Fairbanks. Past warmings are likely to have brought meltwater increases, past coolings meltwater decreases. The latent heat released by these increases and decreases probably amplified the past surface temperature changes.

2.24 Further Simplifications

As in Weertman (1968), Paterson and Clarke (1978), Hooke *et al.* (1980), and Budd and Young (1983), I make the following assumptions to simplify (2.1):

(1) I can treat the problem as two-dimensional. I place the origin at the bed of the ice sheet, define x along the direction of ice flow and z positive upwards. I define u as the velocity component along the flowline and w as the component in the vertical.

(2) The important heat transfer terms are conduction and advection in the vertical direction and advection in the direction of ice flow; the remaining terms are negligible, i.e.: $\frac{\partial^2 T}{\partial x^2} = \frac{\partial^2 T}{\partial y^2} = \frac{\partial T}{\partial y} = 0$.

(3) The ice thickness at Dye 3 has remained constant over time.

With these assumptions, (2.1) reduces to:

$$\rho c \frac{\partial T}{\partial t} = \frac{\partial}{\partial z} K \frac{\partial T}{\partial z} - \rho c u \frac{\partial T}{\partial x} - \rho c w \frac{\partial T}{\partial z} + f. \tag{2.6}$$

To simplify (2.2), I make an additional assumption:

(4) The ice at Dye 3 is incompressible and follows a flow law dependent on the second invariant of the stress tensor (Glen 1958).

I transfer the effects of surface meltwater into the surface temperature forcing as described earlier. Following Paterson and Clarke (1978) and Paterson (1981, c. 3), (2.2) becomes to:

$$f = 2\left[EA_o \exp(Q/RT)\right]^{-1/n} \varepsilon^{(n+1)/n}, \tag{2.7}$$

where ε is an effective strain rate

$$\varepsilon = \left(d_{zz} + d_{xz}\right)^{1/2}. \tag{2.8}$$

and n, A_0, and Q are constants determined from ice creep experiments.

In §7.22, I discuss the consequences of these four simplifications.

2.3 A Simple Heat Flow Model

I will restrict my modelling to the immediate vicinity of the Dye 3 borehole. As a first approximation, I will suppose that the conditions near the borehole control the ice and heat flow required in my analysis. I will model the heat flow at Dye 3 as being one-dimensional. I will suppose that most of the heat flow is along the vertical but I will make corrections for horizontal variations.

A number of recent studies have modelled an ice sheet's heat flow in this way (Budd and Young 1983; Dahl-Jensen and Johnsen 1986; Ritz 1989; Alley and Koci 1990) This approach has its advantages but it also has some severe limitations (§7.22). The details of the simple model are as follows.

2.31 Horizontal Velocity, u(z)

The horizontal movement of an ice sheet affects the temperature in a borehole through strain heating and advection of colder ice from higher elevations (Robin 1955). Hansen and Gundestrup (1988) have determined the horizontal velocity profile at Dye 3 from the tilt of the Dye 3 borehole. Between Dye 3 and the divide near Site Iben, the horizontal surface velocity decreases from roughly 13 to roughly 2 m/a (Reeh *et al.* 1985). The effective surface velocity for the heat flow to the Dye 3 site lies somewhere between these two values. The shape of the profile also probably changes (Raymond 1983; Reeh *et al.* 1985; Dahl-Jensen 1989). I neglect this effect. As a first approximation, I suppose that the velocity profile at Dye 3 applies between Dye 3 and the divide. I make a simple fit of the profile of Hansen and Gundestrup (1988, Fig. 8) to produce the horizontal velocity versus depth curve of Figure 2.2. I average the surface velocities at Dye 3 and Site Iben and make the horizontal surface velocity 8 m/a.

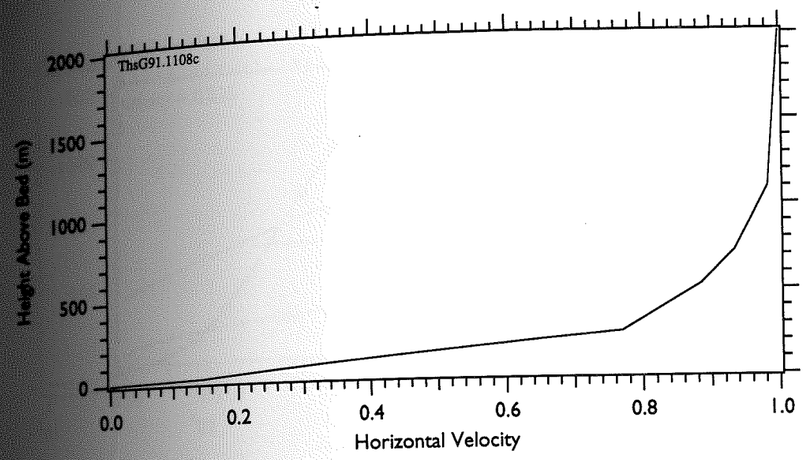

Fig. 2.2 Horizontal velocity profile for Dye 3 based on tilting of the Dye 3 borehole. After Hansen and Gundestrup (1988, Fig. 8).

2.32 Vertical Velocity, w(z)

The vertical movement of an ice sheet affects the temperature in a borehole through strain heating and advection of colder ice from the surface (Benfield 1951; Robin 1955). The thickness of annual layers in the ice at Dye 3 has been determined by ice flow modelling (Reeh *et al.* 1985) and by direct measurement (Hammer *et al.* 1985 1986). These thicknesses can suggest an approximate vertical velocity profile.

I assume the ice along the Dye 3 flow-line flows in two-dimensions (assumption [1]) over a smooth bed. Along the way, I assume the ice maintains a constant thickness, its horizontal velocity follows a fixed profile, and it experiences uniform surface precipitation. Following Nye (1963) and Dansgaard and Johnsen (1969), I can write the horizontal velocity profile as:

$$u(z) = \hat{u}(z)\, c_1 x \tag{2.9}$$

where $\hat{u}(z)$ is the fixed velocity profile and $c_1 x$ is a scaled distance from the divide. Differentiating (2.9) with respect to x and assuming ice is incompressible,

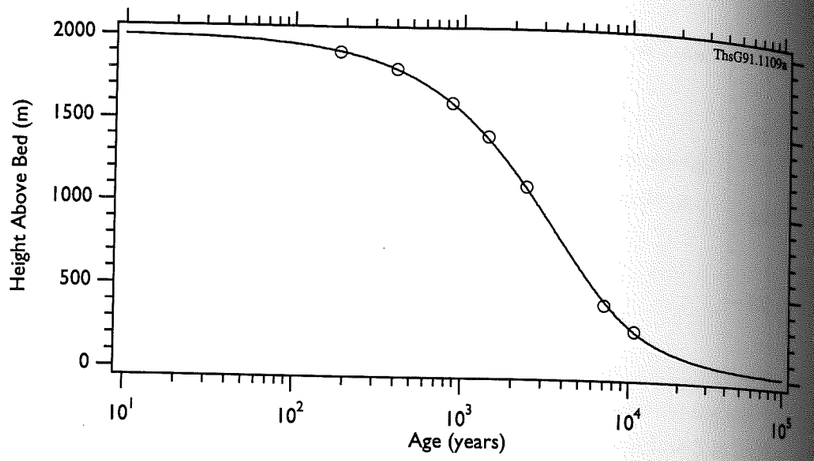

Fig. 2.3 *The time scale for Dye 3 predicted by the model's vertical velocity compared against ages measured at seven depths in the Dye 3 ice core. The former was obtained by integrating the horizontal velocity profile of Figure 2.2 with a vertical surface velocity of 52.5 cm/a, the latter by counting annual layers of dust, oxygen isotope variations, and acidity (Reeh* et al. *1985; Dansgaard* et al. *1989).*

$$\frac{\partial u}{\partial x}+\frac{\partial w}{\partial z}=0, \tag{2.10}$$

I obtain a relation between the vertical and horizontal velocity profiles

$$\frac{\partial w}{\partial z}(z)=-c_1\hat{u}(z). \tag{2.11}$$

I integrate $\hat{u}(z)$ shown in Figure 2.2 to obtain the shape of the vertical velocity profile.

The annual precipitation at Dye 3 is 56 cm/a, decreases to 50 cm/a just upstream of the borehole, and remains near this value past Site Iben and toward the South Dome (Fig 2.1). These precipitation rates are equivalent to vertical surface velocities if I assume that the thickness of the ice sheet has not changed (assumption [3]) and I neglect the small (0.2°) surface slope near Dye 3. I look for a vertical surface velocity within this range to set the scale of the velocity profile.

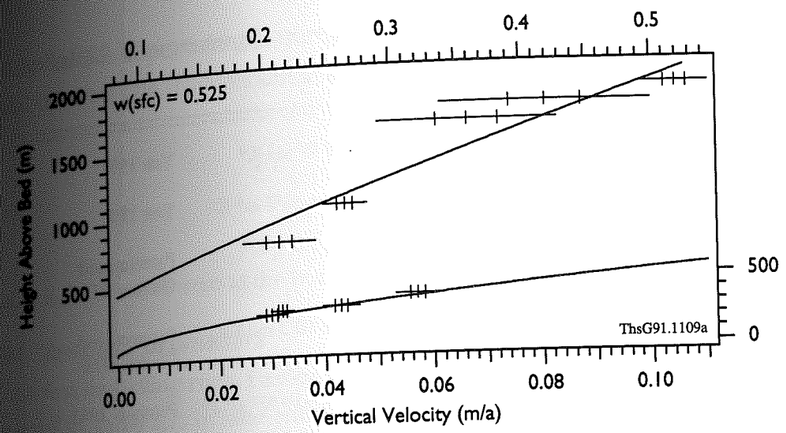

Fig. 2.4 *Annual layer thicknesses for Dye 3 predicted by the model's vertical velocity compared against spot measurements of the Dye 3 ice core (Hammer* et al. *1986, Fig. 1; Hammer* et al. *1987, Fig. 3; Clausen and Hammer 1988, Fig. 3; Hammer 1989, Figs. 3 and 5). Fisher* et al. *(1985) have determined the thickness variations of annual firn layers at Dye 3. The error bars show 50% and 95% confidence intervals (Cleveland 1985, §4.4). Most of the measured layer thicknesses agree with the model within two standard deviations.*

From the vertical velocity profile, I determine the time snow deposited at the surface reaches a particular depth at Dye 3 following

$$t(z)=\int_{sfc}^{z}\frac{1}{w(z)}dz\,. \tag{2.12}$$

I scale the vertical velocity profile by different amounts until I get the best match between the ages obtained through this relation and the age versus depth determined by counting annual layers in the Dye 3 ice core (Hammer *et al.* [1985, 1986]). After a little trial and error, I found that a vertical surface velocity of 52.5 cm/a gave good agreement (R.M.S. error of 3%). See Figure 2.3.

Once obtained, the vertical velocity profile gives direct predictions of annual layer thicknesses. With no further tinkering, I found that a vertical velocity profile with this surface velocity gave predictions in reasonable agreement with spot measurements of layer thicknesses in the Dye 3 core (Fig. 2.4).

Table 2.1 *Parameter values for the first modelling runs. Beginning in §4.22, I allow the parameters marked with a dagger (†) to vary.*

Ice conductivity	K_i	2.257 W m^{-1} K^{-1}	Yen 1981
Ice density/heat capacity	$\rho_i c_i$	1.828 x 10^6 J m^{-3} K^{-1}	Yen 1981
Rock conductivity	K_r	2.5 W m^{-1} K^{-1}	Paterson and Clarke 1978
Rock density/heat capacity	$\rho_r c_r$	1.82 x 10^6 J m^{-3} K^{-1}	Paterson and Clarke 1978
Ice flow law constant	A_0	4.12 x 10^{-12} N^{-3} m^6 s^{-1}	Paterson 1981, c. 3
Ice flow law exponent	n	3	Paterson 1981, c. 3
Activation energy for creep	Q	6 x 10^4 J mole^{-1}	Paterson 1981, c. 3
Surface temperature gradient †	$\frac{\partial T}{\partial x}(sfc)$	0.018 K km^{-1}	Reeh *et al.* 1985; Dansgaard *et al.* 1984b
Geothermal heat flux †	Q_g	41.7 mw/m^2	Firestone *et al.* 1990
Horizontal surface velocity †	$u(sfc)$	8 m/a	§2.31
Vertical surface velocity †	$w(sfc)$	52.5 cm/a	§2.32

ThsG91.1107a

2.33 Horizontal Temperature Gradient, $\partial T/\partial x$

Except very close to an ice divide, the top parts of most ice sheets have a negative temperature gradient, that is their temperature decreases going downward (Paterson 1981, c. 10). This is because the ice flowing to a site is originally deposited on the surface at a colder and higher site upstream.

I include this effect in the model by introducing a horizontal temperature gradient. At the surface, I set it equal to the product of the surface atmospheric lapse rate

and the surface slope. Below the surface, I scale the temperature gradient to the horizontal thinning rate (Dahl-Jensen and Johnsen 1986):

$$\frac{\partial T}{\partial x}(z) = \frac{\partial T}{\partial x}(sfc)\,\frac{\frac{\partial u}{\partial x}(z)}{\frac{\partial u}{\partial x}(sfc)} \tag{2.12}$$

so that it decreases to zero at the bed.

2.34 Various Parameters

In the first modelling runs, I assign values to the model parameters in Table 2.1. In later runs, I allow some of the parameters to vary.

2.35 Numerical Implementation

I solve equations (2.4) and (2.5) using a general purpose, finite-element model that Firestone *et al.* (1990) have applied to heat flow problems at the Summit ice divide, Central Greenland. The full model is capable of solving steady-state or transient problems in two dimensions, with internal heat sources, surface fluxes, and variable material properties. Here, I use a reduced version of the model to solve linear heat flow in one-dimension. I use three-node elements, three-point Guassian quadrature, and a fully implicit time-stepping scheme. I solve for heat conduction and advection in the vertical and I include the effects of strain heating and horizontal heat advection using the velocity patterns and temperature gradient described earlier. Appendix A describes the model's numerical details.

I represent the 2 km of ice and 3 km of rock at Dye 3 by a column of 10 ice elements upon 15 rock elements. I introduce a fixed geothermal flux of 41.7 mW m^{-2} at the bottom of the bedrock. Figure 2.5 shows a schematic of the model.

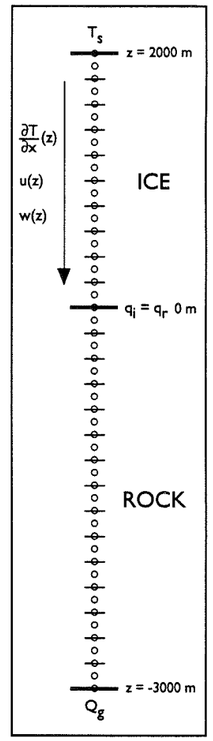

Fig. 2.5 *Heat flow model: nodes and elements, ice and heat flux conditions.*

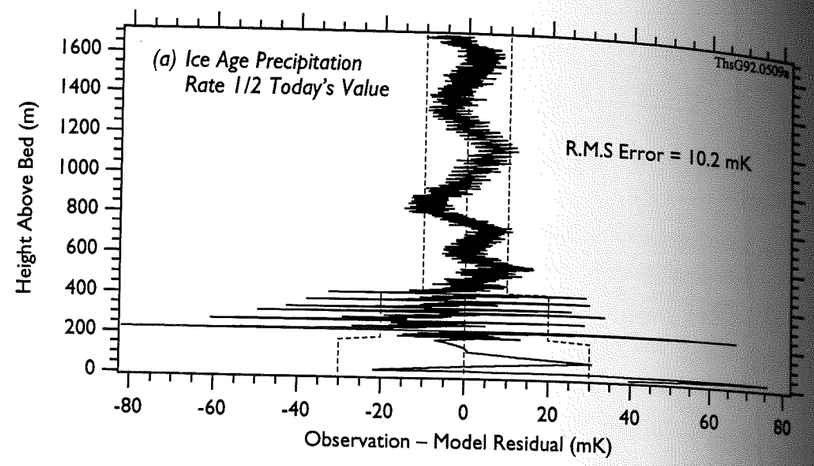

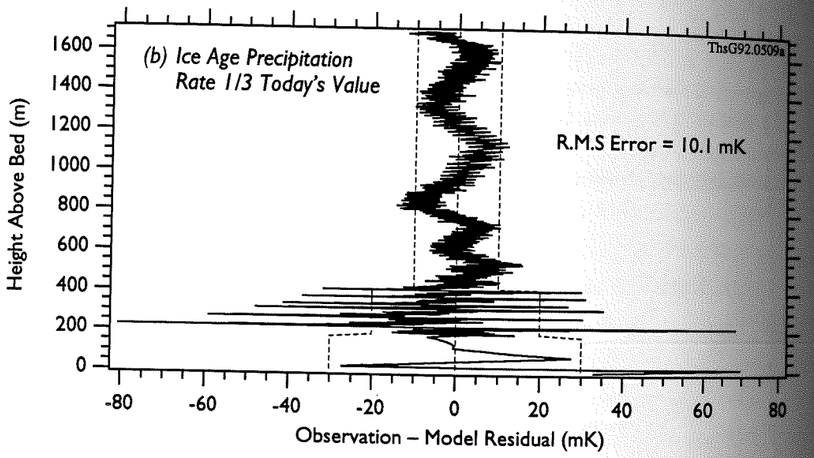

Fig. 6.7a–c *The mismatches between the 1983/1986 Dye temperature observations and the terminal model temperatures produced in the constrained minimizations. The dashed lines show the estimated, best case accuracy of the Dye 3 observations. The mismatch assuming the lowest precipitation rate history shows a larger negative excursion near the surface. Otherwise, the three are quite similar.*

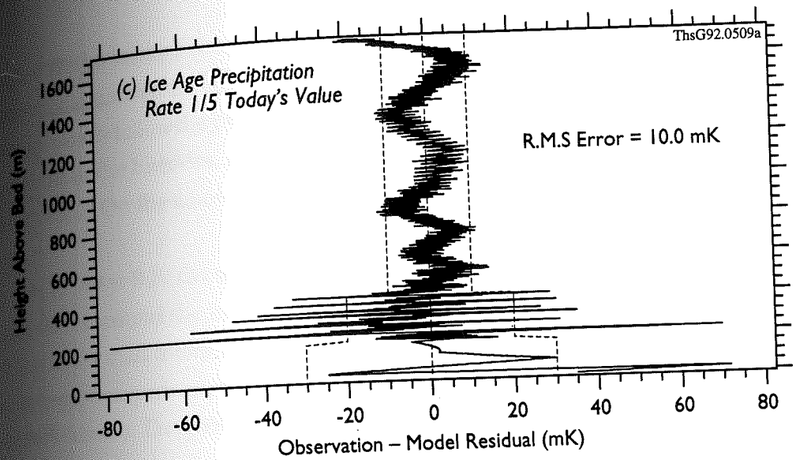

tion histories terminate in 15–18 iterations. This is somewhat longer than in the last, unconstrained minimization which required 13 iterations. The minimizations alternately reduce the preconception and observation mismatches.

Terminal Residuals Figures 6.7a–c show the mismatch of the model terminal temperatures to the Dye 3 observations. Above 200 m height, the residuals are very similar to each other and to the residual obtained in the last minimization. The rapid oscillations and large scale excursions are as in Figure 6.3: nearly all fall within the most optimistic error bands I calculated earlier. There is one last negative excursion near 1700 m, which is stronger for the lower precipitation rate histories.

Below 200 m height, the residuals remain within the 0.03 K error bands, with the exception of the bottom-most peaks which make the 0 and 16 m observations 0.03 and 0.06 K too warm. These may be systematic biases in the model fits, produced by poor physics or numeric ringing from the sharp transition starting at 14 984 yr B.P. The residuals, however, result from just two of the 1983 observations, which may have been biased by the severe instrumentation noise in the 1983 data logging system.

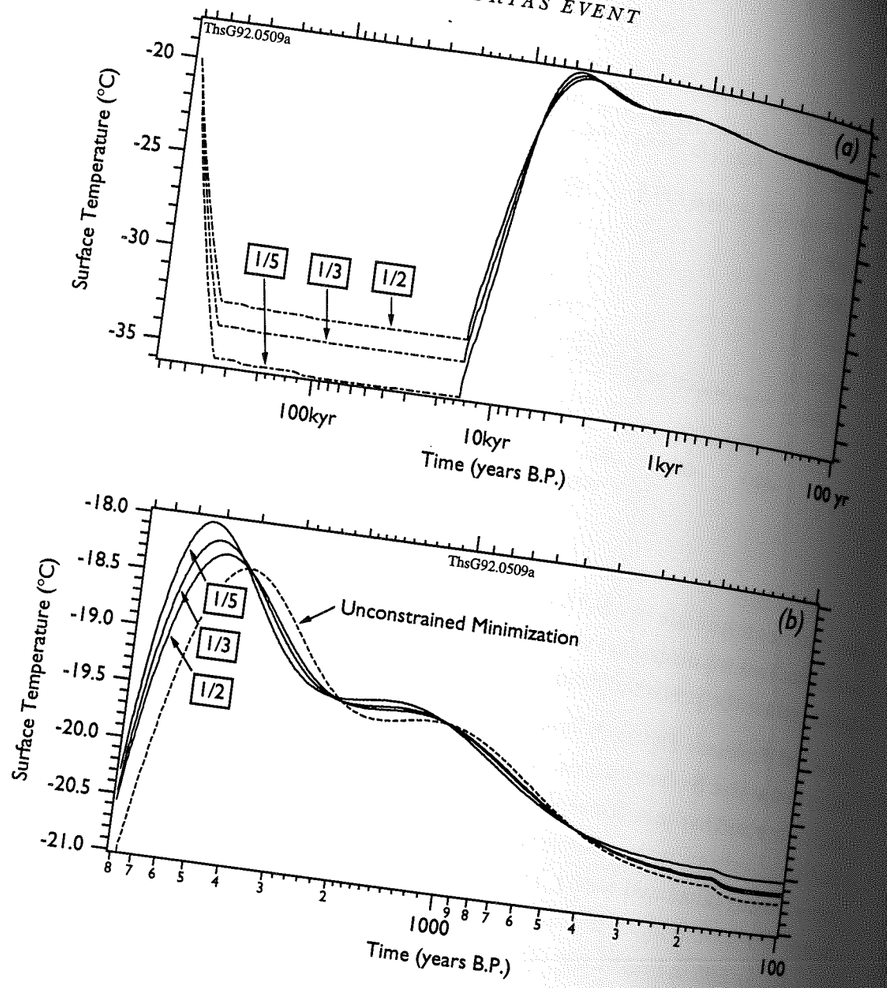

Fig. 6.8a–b *The surface temperature histories equivalent to the surface flux forcings of Figure 6.5. The older portions of the histories (panel a, chained lines) closely follow the forcing preconceptions to their end at 14 984 yr B.P. Panel b shows the more recent portions of the histories in greater detail and also the history determined in the unconstrained minimization. The oscillations and saw-tooth patterns in the surface flux forcings have been largely filtered out. The recent temperature histories are quite smooth and show two sets of peaks. The preconceptions applied to the earlier portions of the histories have shifted the peaks toward older times.*

Surface Temperatures Figure 6.8a shows the equivalent surface temperature histories I obtain for the three ice age precipitation histories. Starting at 675 000 yr B.P., the forcings closely follow the preconceptions to their end at 14 984 yr B.P. There are slight deviations in the histories, most noticeably for the history with precipitation rates 1/5 today's value. On the whole, the surface temperatures are faithful to their preconceptions.

At 14 984 yr B.P., the temperatures jump to warmer values. They reach their maximum values around the time of the Climatic Optimum with peak temperatures 1.8–2.1 K warmer than today. The rapid oscillations in the flux forcing over the transition are strongly damped out. They appear as slight ripples in the slope of the surface temperature history. The peak temperature shifts slightly and changes value depending on the assumed precipitation rate history. It is higher and earlier for lower ice age precipitation rates.

Figure 6.8b shows the recent surface temperatures histories in greater detail. The surface temperature histories following the Climatic Optimum are smooth and similar to what I obtained in the unconstrained minimization. The peak temperatures around the times of the Climatic Optimum and medieval warm period are somewhat older and warmer.

Discussion These simple histories and the simple heat flow model have matched the temperatures measured in the Dye 3 borehole within the smallest error I can expect in their measurement. In the sense that I have produced a simple explanation of the observations, I have succeeded in explaining the temperatures measured in the Dye 3 borehole.

The surface temperature histories show no evidence of a Younger Dryas cooling. This could be because the cooling did not occur. Alternatively, the data sets may contain too little information for the model to detect it. (I can rule out a second alternative, that the data are sufficient but that the model is incapable of detecting the cooling. The test described in Appendix B shows that the model's terminal temperatures are more accurate than the observations.)

6.23 A Minimization with an Added Younger Dryas Cooling

To test the first alternative, that the observations are insufficient, I suppose that the Dye 3 temperature observations indicate that the Younger Dyras cooling had not oc-

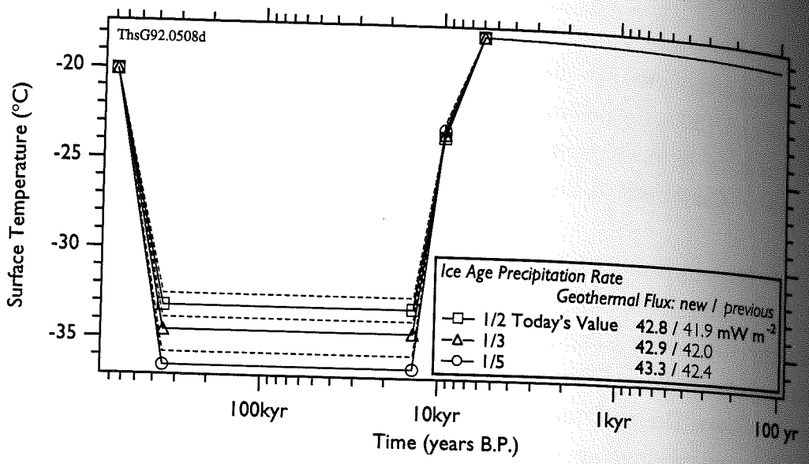

Fig. 6.9 *The geothermal heat flux values and simple surface temperature histories that best match the 1983 temperatures with an added Younger Dryas cooling spike. For comparison, the figure shows the preconceptions determined in §5.3 in light type and with dashed lines.*

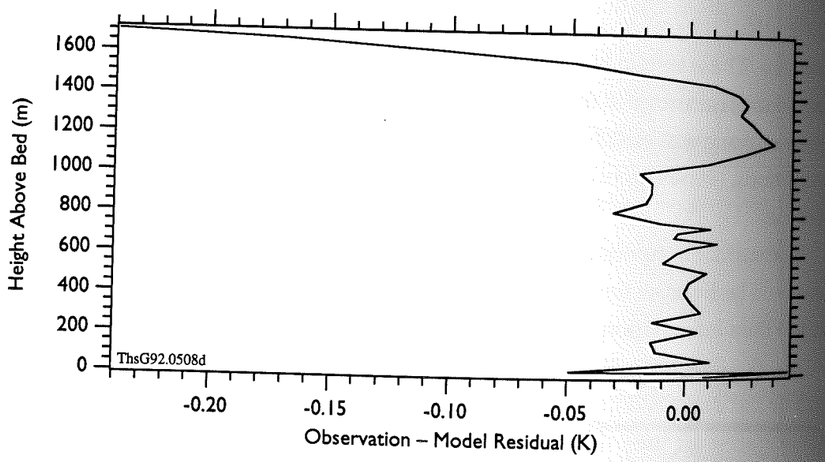

Fig. 6.10 *The mismatch between the 1983 Dye 3 temperature data set with an added Younger Dryas cooling spike and the terminal temperatures produced by any of the six preconceptions of Figures 6.9. By slight adjustments of the geothermal flux values and ice age temperatures, the new preconceptions have removed nearly all traces of the added Younger Dryas cooling spike.*

cured. I run the heat flow model once more without heat strain heating, a geothermal heat flux, or horizontal advection. I apply to the model a 7 K surface temperature spike between roughly 11 500 and 10 700 yr B.P. I obtain the cooling that would have been added to the Dye 3 borehole temperatures had the supposed cooling during the Younger Dryas occurred.

I add this response to the combined temperature data set, run more minimizations and try to detect this cooling. First, I compute a set of preconceptions following the procedure of §5.3. Figure 6.9 shows the temperature histories and geothermal flux values I obtain and compares them to those from the previous preconceptions. According to the figure, had something like a Younger Dryas cooling occurred, the geothermal flux value would have been roughly 1 mW m^{-2} higher; while the surface temperatures would have been 1 K cooler during the ice age temperatures, 0.4 K cooler at 9624 yr B.P., and largely unchanged at later times.

Figure 6.10 plots the residuals from the preconceptions with and without the supposed Younger Dryas cooling. To the accuracy at which I can draw lines on the page, they are identical.

With just the minor adjustments to the preconceptions shown in Figure 6.9, I have produced nearly identical matches to the Dye 3 temperature observations. The final preconceptions give no hint of a Younger Dryas cooling. There is little point in running a detailed minimization. With these minor adjustments the new preconceptions have removed any residual that might have been left by a Younger Dryas cooling.

I can only conclude that I can not detect the Younger Dryas event with the Dye 3 temperature measurements.

CHAPTER SEVEN

Prospects

If the temperatures in the Greenland ice sheet show any remnants of a Younger Dryas cooling, those remnants will be subtle and difficult to distinguish from measurement and modelling errors. To identify the remnants in a set of borehole temperatures, and so say something about the Younger Dryas, will require more accurate measurements, better models, and a more refined analysis than those I used in Chapter 5.

On the first two counts, Dye 3 is not an ideal site to detect and resolve the Younger Dryas event. It always shows some surface melting in the summer, which complicates the surface heat forcing (§2.23) and disturbs the ice stratigraphy (Dansgaard *et al.* 1984b); it is far from the ice divide, which requires "elevation" corrections in the isotope and heat flow analyses (*Ibid.;* §2.33); it has very rough bedrock topography upstream which limits the modelling of its ice flow (Reeh *et al.* 1985); and it has a high accumulation rate which advects much of the remnants of temperature changes during the Younger Dryas into the bed below the ice sheet (Fig. 2.8). For these and other reasons, investigators have looked to Central Greenland for more favorable drilling sites (Dansgaard *et al.* 1982; Clausen *et al.* 1988).

Two groups are now drilling a pair of deep holes at and near the Summit ice divide in central Greenland (lat. 72° 18' N., long. 37° 55' W). The GRIP European and GISP II American projects expect to reach bedrock in the summers of 1992 and 1993 and to retrieve two detailed ice cores dating back several glacial cycles. Extensive geochemical analyses of the cores are now underway, and to better interpret the cores, geochemical and geophysical surveys around the drilling sites have been undertaken, are in progress, and are planned. On all accounts, our understanding of the geophysics and geochemistry at Summit and its past climatic change will surpass what we know or could know from Dye 3.

The temperatures of the partially-completed GRIP borehole have already been measured (Gundestrup *et al.* unpublished, Dome Grip) and more detailed and accurate surveys are planned. What are the possibilities that these measurements might detect the Younger Dryas event in Greenland? In this chapter I will try to answer that question by determining the measurements, models, and analysis that are required.

7.1 Observation Requirements

The borehole temperature response to the Younger Dryas has had thousands of years to diffuse. Detecting the Younger Dryas in the present day borehole temperatures will require accurate temperature measurements. The temperatures I tried at Dye 3 were not accurate enough.

7.11 An Identical Twin Experiment

I conduct an *identical twin* experiment to determine the minimum observation accuracy required to identify the Younger Dryas event at Summit. I construct a model with conditions like at Summit, I run the model with a simple Younger Dryas cooling history and I obtain a set of terminal temperatures which I call the "observations." I minimize as before and I obtain a surface temperature history that best matches these synthetic observations. A sufficiently accurate model and proper procedures should produce a history from the "observations" that is an identical twin of the original.

General Model and Solution For the experiment, I adapt the model and optimal control methods of Chapter 5. To concentrate on the forcing most relevant to the Younger Dryas problem, I set the geothermal flux to zero and only try the median precipitation history with a minimum ice age precipitation rate 1/3 today's value. To keep the experiment simple, I model the approximate ice and heat flow at the ice divide and I ignore strain heating as its contribution to the temperature field is independent of the surface temperature.

Assumed Velocity Field I use for my velocity field, vertical velocities produced by a steady-state, two-dimensional, finite element model for Summit (Schøtt *et al.* 1992). I assume, as does the model, a linear variation between the nodal velocities given in Table 7.1.

Spatial Mesh I represent the 2968 m of ice and 3000 m of rock at Summit using the same mesh as at Dye 3 (Fig. 4.7), stretched to the Summit geometry. To improve the accuracy of the modelling, I increase the number of nodes and elements by ten times, to 246 elements and 493 nodes. Since the heat flow model does not account for the variable thermal properties of firn, in my analyses, I disregard the temperatures over the first 100 m depth.

Time Mesh Using a spatial mesh 2.5 times less dense, I repeat the pulse sensitivity tests of §3.1 and §3.2 to determine borehole responses and the shortest detectable temperature pulses at Summit. Figure 7.1 shows the responses to surface temperature step changes. At Summit, surface temperature changes at take longer to propagate into the ice sheet than at Dye 3 (Fig. 3.1). The half-response to a step change applied around the time of the Younger Dryas just reaches the middle of the ice sheet, while at Dye 3, the half-response nearly reaches the bed.

Figure 7.2 shows the shortest detectable pulse widths for a pulse applied at Summit between 0 and 675 000 yr B.P. Compared to Dye 3, the minimum detectable pulse widths at Summit are shorter and more sensitive to the precipitation rate pattern. This is true at more recent times, because I include in the analysis temperatures closer to surface, and for more ancient times, because the response to a surface temperature change takes longer to propagate into the ice sheet.

To keep computing expenses and running times to an acceptable level, I ignore heat flow at older times. I apply the analysis of Appendix B to establish a set of time steps between 30 000 and 0 yr B.P. I limit myself to 2000 time steps. To eliminate the saw tooth noise that appears in Chapter 6, I dispense with the time knot scheme of §B.2 and fit 2000 time steps of equal influence to the $\sigma = 0.01$ curve of Figure 7.2. Figure 7.3 shows the time steps I obtain.

Younger Dryas History and Response In §6.23, I found that a modest adjustment of the ice age temperatures, too modest to be distinguished by the Dye 3 isotope record,

Table 7.1 *The vertical velocities assumed in the Summit model. From Schøtt et al. (1992).*

Height Above Bed	Vertical Velocity
2968 m	0.231 0 m/a
2330	0.155 6
1932	0.111 2
1592	0.077 23
1285	0.050 59
1001	0.030 28
733.2	0.015 44
478.7	0.005 842
234.8	0.001 137
0	0

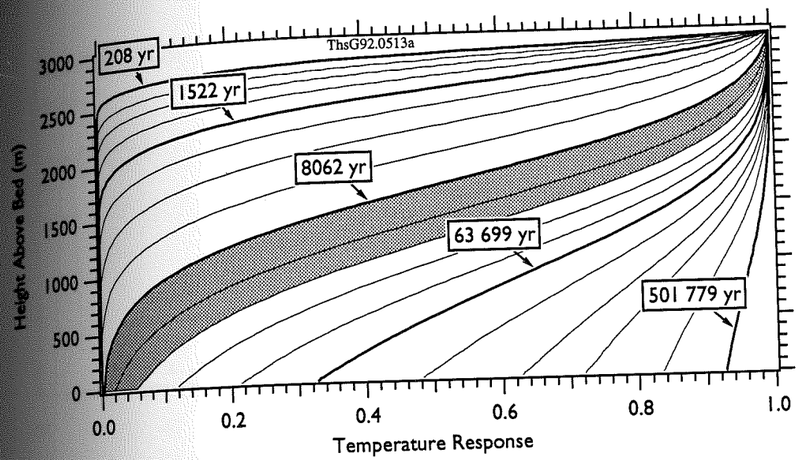

Fig. 7.1 The present day, Summit borehole temperature response to a step change in surface temperature applied at ***208****, 416, 649, 996,* ***1522****, 2317, 3516, 5327, 8062, 12 199, 18 447, 27 886, 42 148,* ***63 699****, 96 262, 145 459, 332 095, and* ***501 779*** *yr B.P. The responses appear at greater heights than at Dye 3 (Fig. 3.1). The shaded region shows the responses from roughly the last deglaciation.*

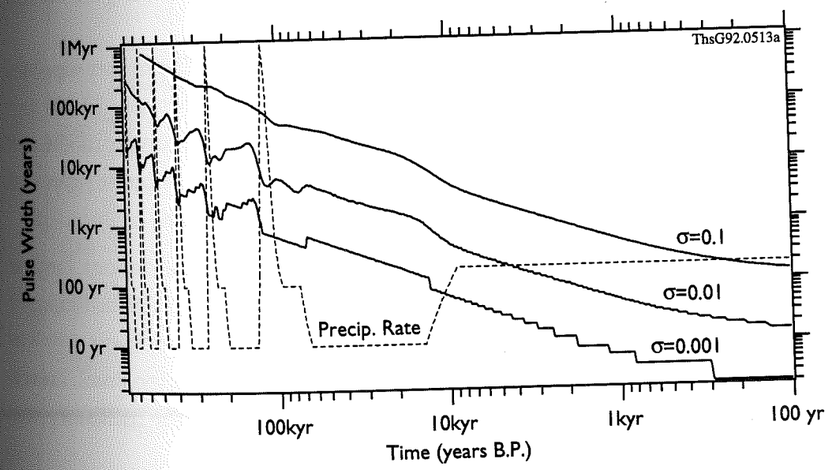

Fig. 7.2 The shortest surface temperature pulse detectable in the Summit borehole temperatures at observation noise levels of 0.001, 0.01, and 0.1. The three curves assume the precipitation history of Figure 2.6 (dashed line) and criterion (3.2). The shortest detectable pulse widths are shorter at Summit than at Dye 3 (Fig. 3.4).

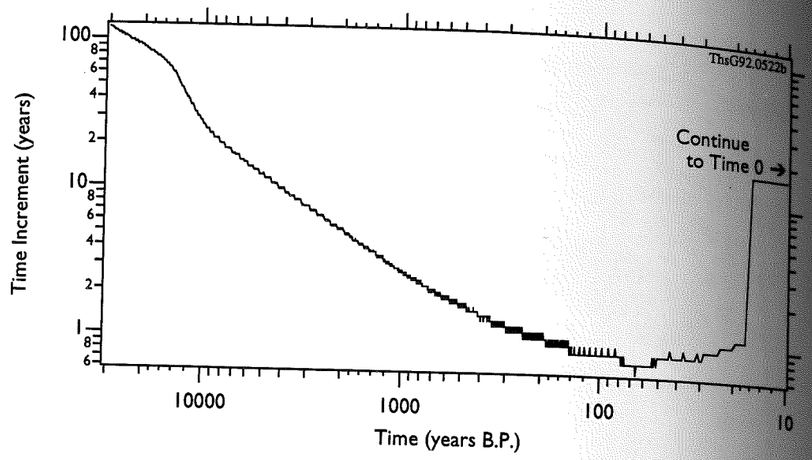

Fig. 7.3 The spacing and placement of the 2000 Summit model time steps determined from Figure 7.2.

would remove the response left by a Younger Dryas cooling. I wish to test this possibility at Summit. I therefore include in the history both a Younger Dryas cooling and ice age temperatures.

I apply to the model a history similar to Scenario B of §1.32. The history supposes a present day temperature of -32.3 °C, a Younger Dryas cooling between 11 500 and 10 700 of 7 K, and an ice age temperature 13 K colder than today. I run the model and obtain a response in the Summit borehole. Figure 7.4 shows the response separated into its ice age temperature change and Younger Dryas cooling pulse components.

Recovered Surface Temperature Forcing With this response as my observations, I repeat the minimization procedure of §5.5 and try to recover the Younger Dryas forcing. I first assume no preconception (apply no regularization) and seek the closest match to the "observations." After 25 iterations (and three days of Sun Sparcstation time), I reach a minimum matching the response within 10 μK. Figure 7.5 shows the oscillatory mismatch I obtain.

Figure 7.6 shows the twin surface temperature histories: the history that created the observations and the scenario I recover from them. The recovered scenario is a smooth copy of the applied history. The scenario begins and ends with a cycle of what

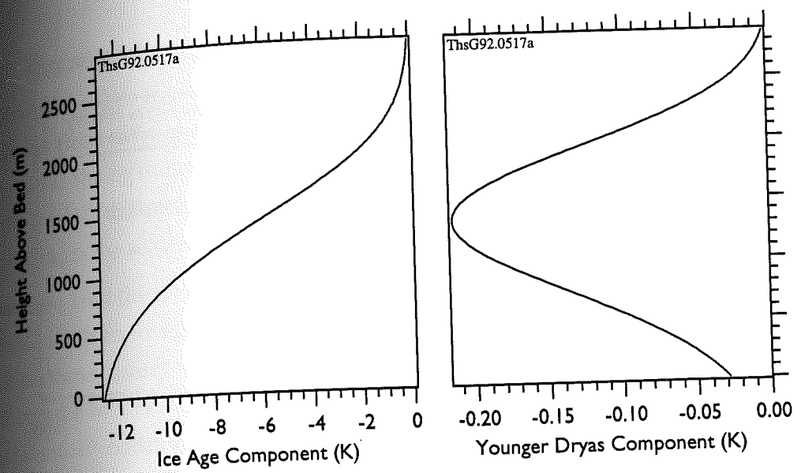

Fig. 7.4 The present day temperature response left in the Summit borehole by a temperature scenario similar to Scenario B of Figure 1.8.

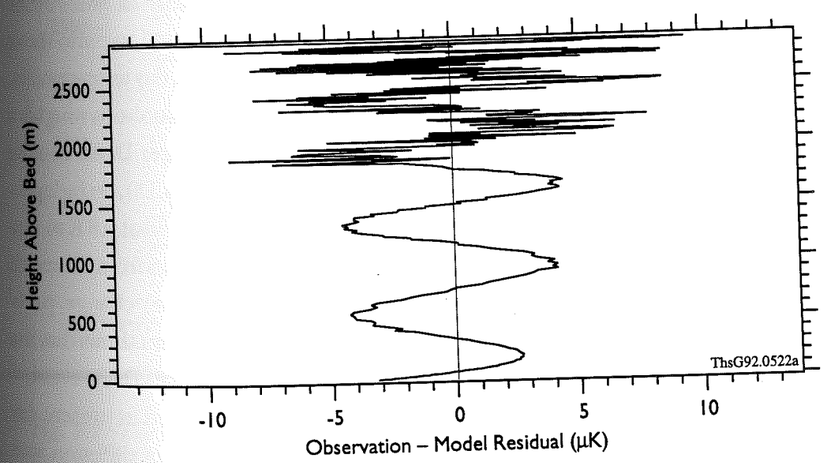

Fig. 7.5 The mismatch between the synthetic Summit temperature observations and the terminal model temperatures produced in the Summit identical twin test.

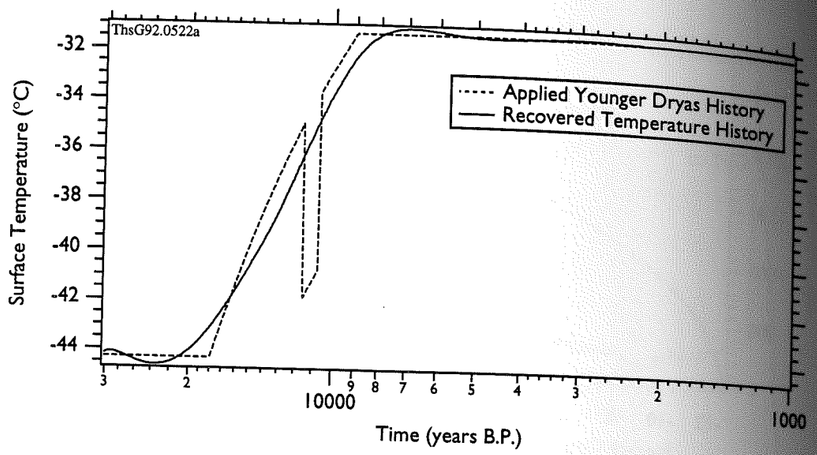

Fig. 7.6 The Younger Dryas cooling history that produced the synthetic Summit borehole observations and the recovered temperature history whose terminal temperatures most closely matches them. Modest Gibbs's oscillations appear in the history before and after the ice age/interglacial transition. The history shows little or no hint of the Younger Dryas cooling spike.

are probably Gibbs's oscillations. Despite the extremely close match to its twin's terminal temperatures, over the glacial–interglacial transition, the recovered scenario shows no changes more rapid than the slow change from ice age to present day temperatures.

Between roughly 15 000 and 9000 yr B.P., the recovered scenario shows roughly a 0.9–1.4 K cooling. Otherwise, it gives little or no hint of the Younger Dryas cooling spike. Based on the scatter of recent $\delta^{18}O$ values from Greenland (§4.13), an independent temperature history would have to demonstrate a change of at least 0.8 K to support or deny recent events recorded in the Dye 3 $\delta^{18}O$ record. For events from the much less certain ice age, a temperature history would have to show a greater change, probably at least twice this value. On that basis, the identical twin experiment shows that the model I have just constructed is incapable of distinguishing a Younger Dryas event.

Diffusion of some kind, either physical or numerical, has removed its present day response. The model's finite accuracy introduces a certain amount of diffusion into the temperature calculations. It is quite possible that this diffusion is greater than the physical diffusion at Summit.

7.12 The Model's Numerical Diffusion

The model solves the heat flow equations at a fixed number of points on a finite element/finite difference mesh. This discretization of the continuous heat flow field can lead to strong numerical diffusion. A quick and easy way to tell if this is the source of the model's diffusion and then to judge its effects is to refine the mesh and see how that changes the solution.

Procedure I test the mesh refinements using two histories: the history used in the minimization with an ice age temperature step change and a Younger Dryas cooling pulse, and the same history with just a Younger Dryas cooling pulse. I apply the first history and run the heat flow model with 2000 time steps and a finite element mesh with ten times as many nodes and elements. I apply the second history and run the model with 2000, 6000, and 20 000 time steps.

Diffusion Introduced by the Spatial Mesh Figure 7.7 shows the changes in the terminal model temperatures after increasing the number of nodes and element by ten times.

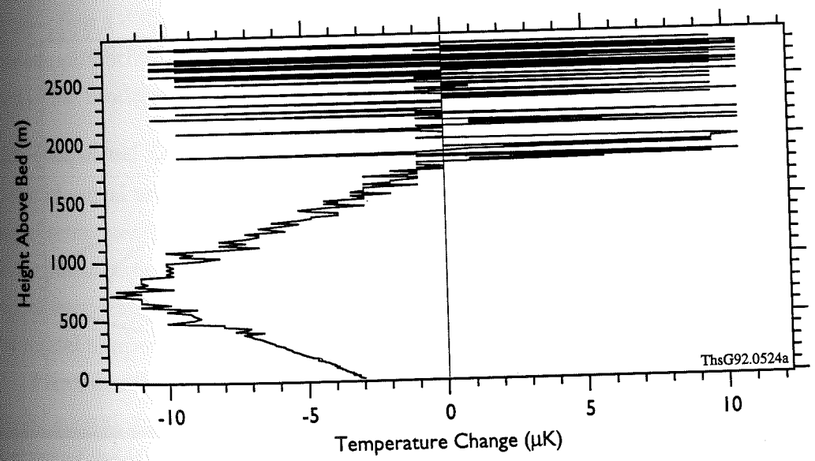

Fig. 7.7 The changes in the Summit borehole temperatures after increasing the number of spatial elements and nodes by ten times. The changes above 1800 m are similar to the observation–terminal temperature residuals obtained in the minimization. The changes below probably show the discretization error of the original spatial mesh.

The changes are of similar magnitude and pattern as the mismatch I obtain in the minimization. (Fig. 7.5). The changes show a simple excursion reaching 12 μk at 700 m. In other regards, the changes are unremarkable. The finite element mesh is probably only a minor source of the model's diffusion.

Diffusion Introduced by the Time Stepping Scheme Figure 7.8 shows the fractional change in the present day Younger Dryas response after increasing the number of steps from 2000 to 6000 and from 2000 to 20 000. Increasing the number of time steps slightly shifts, strengthens, and sharpens the response. In the minimization, I tried a history that included a Younger Dryas cooling spike, but I could not recover it. Since the response to the spike sharpens as I increase the number of model time steps, the diffusion within the present model probably can not be explained by physical causes.

The root mean square differences between the responses using 2000 and 6000 steps and between the responses using 6000 and 20 000 steps are 1.8 mK and 0.6 mK, respectively. These differences follow the linear decrease in error with time step size of a fully-implicit, backward difference, time-stepping scheme. This strongly suggests that

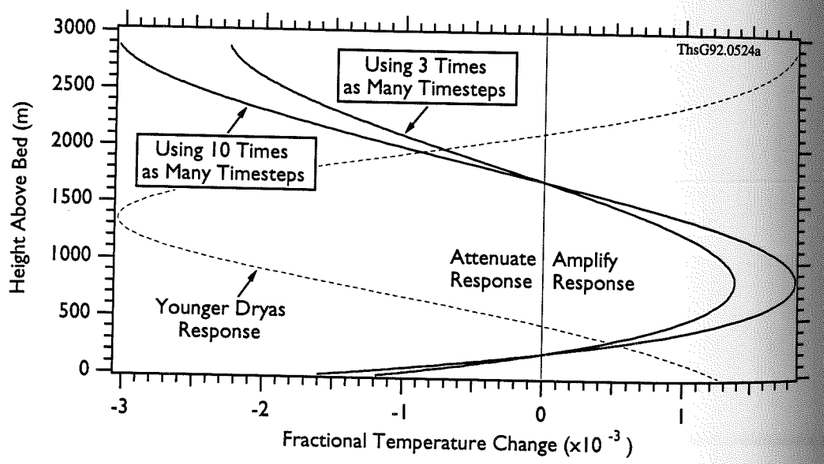

Fig. 7.8 The changes in the Summit borehole temperatures after increasing the number of time steps by three and ten times (from 2000 to 6000 and from 2000 to 20 000 time steps). Increasing the number of time steps amplifies, sharpens, and slightly shifts the Younger Dryas response. These changes are consistent with diffusion introduced by the implicit time-stepping scheme.

the diffusion within the model is largely numerical—from the implicit time-stepping scheme.

Such a scheme is said to be *consistent* with the transport equation I am solving (Noye 1982). I can expect that as the time step size decreases, the model's finite difference solution will approach the solution of differential heat flow equations. For some sufficiently small time step size, I can expect the diffusion from time-stepping will become less than the physical diffusion. At present, the model's numerical diffusion is greater.

If I project the response differences for 2000, 6000, and 20 000 time steps, I estimate that the 2000 steps taken in the minimization introduce an error of 3 mK into the terminal temperatures. I can view this as modelling "noise" introduced by the time-stepping. Other possible sources of modelling noise are the discretization error of the spatial mesh and round off error in solving the linear equations for the heat flow physics. I have increased the size of the spatial mesh and found that this had a much smaller effect on the terminal temperatures. I solve the linear equations to sixteen significant figures. Assuming something other than a very poorly-conditioned set of equations, this implies a still smaller error. If I suppose there are no other sources of modelling error—often a difficult and subtle proposition with numerical models—the model's time-stepping scheme will be the chief source of modelling noise. In that case, the noise level of the model is about 3 mK.

7.13 Required Observation Accuracy

In the identical twin experiment, the synthetic observations are themselves terminal model temperatures. This implies that the observations contain about 3 mK of noise. In the minimizations, the terminal model temperatures are not used alone; rather, the model temperatures are always differenced with the observations. This difference, not the model temperature, is what really "drives" the minimizations.

I have concluded that I can not distinguish the Younger Dryas event because the model adds about 3 mK of noise to the terminal model temperatures. From the perspective of the identical twin test, I can just as well conclude that I can not distinguish the event because the observations have about 3 mK of noise. Suppose I were to improve the model so that the noise in the terminal model temperatures was a great deal smaller. The test suggests that the Younger Dryas event could not be distinguished in

the temperatures observed at Summit unless the temperatures are measured to a greater accuracy.

The observation accuracy actually required will be related to the amount of physical diffusion. I have not considered the level of thermal diffusion in the Greenland ice sheet beyond noting that it is much less than the model's numerical diffusion. Diffusion melds information. The greater numerical diffusion in the present model must exaggerate the difficulty in resolving the Younger Dryas event at Summit.

Given that the physical diffusion at Summit is less, with a better model, we may not have to measure temperatures in the Greenland ice to within 5–10 μK (the final residuals obtained in the identical twin test). Nevertheless, the model in the identical twin tests does calculate terminal temperatures to within 3 mK or so. To distinguish the Younger Dryas event from the temperatures observed at Summit will require temperature measurements considerably more accurate than 3 mK, but not necessarily as accurate as 5–10 μK.

7.2 The Model Required

The finite element model I use includes what are probably the important heat flow physics at Summit. With its surface precipitation history and velocity field pattern, the model also tries to include the effects of the important ice flow physics as well. Details in the physics that the model omits or glosses over will increase the error of the model's terminal temperatures. This error will need to be reduced to the error of the Summit borehole observations if heat flow modelling is to give a meaningful pronouncement on the Younger Dryas cooling. Supposing the temperatures in the Summit borehole can be measured to a greater accuracy than 3 mK, I can use this handy figure to determine some minimum requirements for a model that might distinguish the Younger Dryas event at Summit.

7.21 Improved Numerics

First of all, the model will need to introduce less numerical diffusion into the calculations than occurs through the physical diffusion operating at Summit. The model's time stepping scheme must be made more accurate. This is straightforward. The

model's fully-implicit, backward difference time-stepping scheme can be replaced with a much more accurate, second order Crank–Nicolson method (Noye 1981).

7.22 Additional Physics

Firestone *et al.* (1990) have modelled the heat flow at Summit to determine if basal melting has occurred at the GRIP and GISP II drill sites. In modelling the temperature under the Summit ice divide, they conducted a series of sensitivity tests of increasingly complex heat flow models. I will use their model results to determine the additional physics that need to be added to the simple heat flow model.

The model and forcings of Firestone *et al.* are similar to those I use in the present work. My simple heat flow model is derived from theirs and differs chiefly in being one-dimensional rather than two and integrating over each element using full rather than reduced Gaussian quadrature (three points per dimension instead of two). In applying their model, Firestone *et al.* took time steps of fixed size, used less refined vertical velocities, and found solutions on a coarse vertical grid of only ten elements. The temperature and precipitation forcings they applied are similar to Figure 2.6; that is, their forcing changes are of thousands of years duration. Their model solutions will thus lack the effects of shorter term variations. I will use their results to first determine the minimum model required to model longer term changes.

The next two figures show results from their forcings and models. Figures 7.9 and 7.10 show how the ice sheet temperature profiles change as various complications are added to the heat flow physics.

Temperature Dependent Thermal Properties The right-most curve of Figure 7.9 shows the effects of making the ice sheet's thermal conductivity and diffusivity temperature-dependent. Warm temperatures at depth increase the thermal conductivity and decrease the average temperature gradient between the surface and the ice sheet's bed. This reduces the temperatures near the bed. Approaching the surface, colder temperatures decrease the conductivity and increase the gradient, leading to warmer temperatures at mid-level. This is a complex change of several degrees which changes most rapidly at mid-level, the height showing the peak response of a Younger Dryas event (dashed line). An ice flow model would need to include this non-linearity in the ice sheet's thermal properties to accurately model these changes.

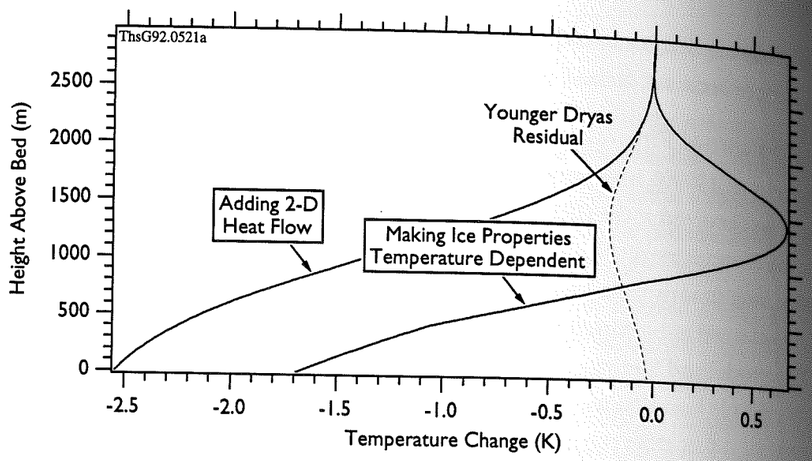

Fig. 7.9 The changes in the Summit borehole temperatures obtained by Firestone et al. *(1990) after making the ice conductivity and diffusivity temperature dependent and after making the heat flow two-dimensional.*

Two-Dimensional Heat Flow The left-most curve of Figure 7.9 shows the effects of making the ice sheet's heat flow two-dimensional. Horizontal heat flow diffuses away the thermal "hot spot" caused by reduced vertical ice velocities at the divide. The temperatures become colder, increasingly so approaching the bed. This is a larger and more gradual change, but the heat flow model would need to include it to model temperatures more accurately than 3 mK.

Moving Ice Divide These last two curves show results for heat flow at the present day Summit ice divide. It is possible, however, that the ice divide may have migrated by up to 50 km between glacial and interglacial times (Reeh 1984). Figure 7.10 shows the effect on the temperature profile of moving 3 and 10 km off the divide (roughly 1 and 3 ice thicknesses). These small movements of the divide cause complicated and time-dependent patterns of cooling. The heat flow model would have to include these effects if the ice divide has only recently moved to its present position.

Precipitation Rate Changes The work of Firestone *et al.* and the present work assume a particular simple, slowly changing precipitation history. Precipitation rate changes can

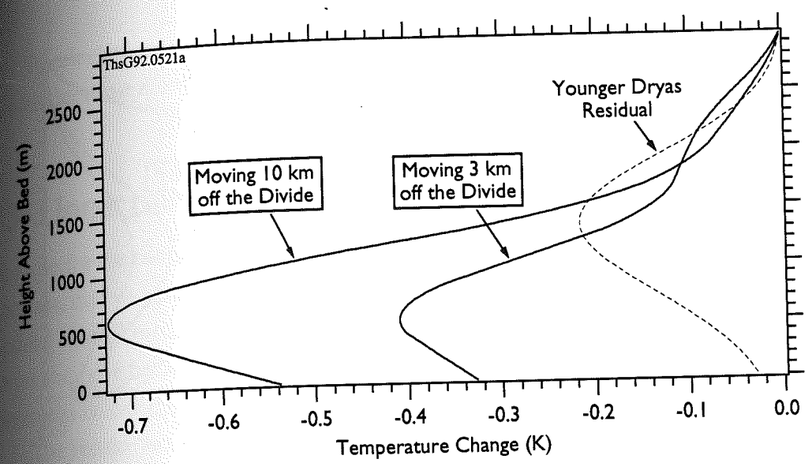

Fig. 7.10 The changes in the Summit borehole temperatures obtained by Firestone et al. *(1990) after moving 1.0 and 3.3 ice thicknesses off the divide (3 and 10 km). The cooling peaks at depth show the diminishment of the basal "hot spot" away from the divide.*

significantly influence the temperatures within an ice sheet as, for example, I demonstrated in the minimum surface temperature pulse width analysis of §3.24. Dansgaard *et al.* (1989) have analyzed the 1786 m portion of the Dye 3 ice core believed to record the end of the Younger Dryas event. Based on their analysis of the changes in dust content, δD, and $\delta^{18}0$ values, they believe the precipitation rate roughly doubled at the termination of the Younger Dryas event.

To test the effects of a short precipitation rate change, I rerun the simple heat flow model and Younger Dryas history of §7.11. I cut the precipitation in half for 835 years during the Younger Dryas, for 835 years 2000 years before and 2000 years after. Figure 7.11 shows how these cuts change the present day temperatures. In these instances, reducing the precipitation rate has an effect on the borehole temperatures similar to, but less severe than, decreasing the surface temperature by 7 K. The model would have to consider the effects of short term precipitation rate changes such as these.

Time Dependent Ice Flow The simple model supposes a simple velocity pattern has existed at Summit at all times. This is unrealistic in two important ways.

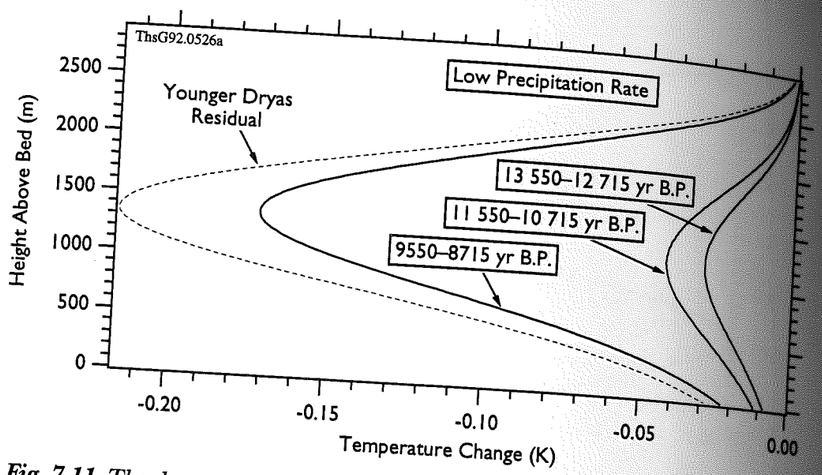

Fig. 7.11 *The changes in the present day Summit borehole temperatures after halving the precipitation rate between the times shown. In this example, the effect is similar to decreasing the surface temperature around those times.*

First, this assumes that the ice sheet's heat and ice flow have no effect on one another when, in reality, they are coupled through the velocity terms in the heat flow equation and the variation of ice rheology with temperature. The rheology of ice changes rapidly as its temperature nears the melting point. This must influence the velocity pattern, especially near the bed, where temperatures at times approach the melting point and the bulk of the ice sheet's deformation occurs. If the velocity and temperature were fully coupled and mutually consistent, the borehole temperatures at Summit would be altered in a complicated way though by an amount less than 2.5 K (Firestone *et al.* 1990).

Second, the simple velocity pattern assumes the ice sheet's thickness has not changed over time. This probably exaggerates the influence of precipitation rate changes on the terminal borehole temperatures. The central Greenland ice sheet was perhaps 100 to 150 m thicker during the last ice age (Reeh 1984; Létreguilly *et al.* 1991). This change would introduce different surface-temperature boundary conditions and alter the stresses controlling the ice velocity pattern. The net effect on the terminal temperatures is again complicated and unknown.

To calculate temperatures to an accuracy better than 3 mK, a model would have to consider these effects of time dependent ice flow.

7.3 Uncertainty Analysis

Suppose, for the moment, that we obtain borehole temperature measurements of high accuracy, that we construct a model faithful to the heat flow at Summit, and that by optimal control methods we obtain results that suggest something about the Younger Dryas. Suppose further, that we have made those results as simple as possible. To make the results convincing, we still need some way to determine their uncertainty.

The results, once we obtain them, will require a better analysis than I have given here. The tests of Chapter 3 estimated the sensitivity of the present day Dye 3 borehole temperatures to past surface temperature changes. They showed that cooling during the Younger Dryas might be detectable in the present day borehole temperatures. These sensitivity tests had a very practical use: they suggested a set of time step sizes for the minimizations that produced simple, smooth forcing solutions well into the last ice age. The need to regularize the solutions over the last ice ages suggests what the sensitivity tests have not shown, the uncertainties of the solution in matching the observations.

At Dye 3, it was not necessary to have a precise or even rough idea of the forcing solution uncertainties. A modest and extremely simple adjustment of the forcing was enough to remove the residual of a Younger Dryas cooling. When conditions are more favorable, when we have created better models, obtained more accurate observations, and determined solutions with specific details about the Younger Dryas, we will require more precise estimates of the solution uncertainties. An analysis using the Hessian of the performance function will give those estimates.

If we ignore for the moment the workings of the optimal control machinery, I can describe the minimizations of the last few chapters as little more than finding parameter values that produce a best least squares fit to a set of observations. If I suppose, as in §4.21, that the observations have random, normally distributed errors, then I can estimate confidence intervals for each model parameter using the inverse Hessian of the performance function. If I define the performance function as a composite function of the flux forcings and all other dependent variables,

$$L' = L'\left(\mathbf{Q}_f, \mathbf{y}\right), \tag{7.1}$$

the Hessian of the performance function will be

$$\mathbf{H} = \frac{1}{2}\sum_{i=1}^{M+1}\sum_{j=1}^{M+1}\frac{\partial^2 L'}{\partial Q_f(i)\partial Q_f(j)}Q_f(i)Q_f(j). \tag{7.2}$$

The condition number of the Hessian measures the general error of the solution (Gill *et al.* 1981) while the inverse of the Hessian gives the covariance of the chi-squared fit of the model to the data (Press *et al.* 1986; Thacker 1989). By the relation

$$\Delta Q_f(m) = \pm\sqrt{\Delta\chi^2}\sqrt{H^{-1}_{mm}} \tag{7.3}$$

these covariances can provide confidence intervals, $\Delta Q_f(m)$, for each forcing parameter, $Q_f(m)$ (Press *et al.* 1986, §14.5).

The Hessian of the performance function can be determined in a number of ways (Thacker 1989). Most straightforward, but rather inefficient, would be to obtain its second derivatives by taking finite differences of the sensitivities produced by the adjoint trajectory. That would involve: perturbing each of the model forcings, running the forward model (5.11) to obtain mismatches to the data, running the adjoint model (5.16–5.18) to obtain the gradient of the performance, and then taking divided differences.

7.4 Discussion

To distinguish the Younger Dryas event at Summit will require better observations, better models, and better uncertainty analyses. What are the prospects of improving all three so that we may distinguishing the Younger Dryas event at Summit?

The Prospects for Accurate Observations The observations required will have to be much more accurate than 3 mK. The current "state of the art" in borehole temperature logging is around 1 mK accuracy. The temperature loggings at Dye 3 can suggest some of the difficulties of achieving higher accuracies. The temperature gradient near the bed at Dye 3 is around 1 K per 100 m. For a probe to measure temperatures near the bed accurate to, say 300 mK, will require knowing its position within a few tens of centimeters and establishing good thermal contact with the surrounding ice. The loggings at

Dye 3 had estimated height errors of 1.5 m and showed 0.1 K jumps in temperature caused by convection cells in the borehole fluid. Neither problem is likely intractable, but solving either will take some effort. To this modeler at least, it does not seem impossible to get sufficiently accurate observations.

The Prospects for an Accurate Model The model that analyzes these observations will have to be more accurate and complete. Replacing the heat flow model's implicit time scheme with a Crank–Nicolson method will make the scheme sufficiently accurate. To be sufficiently complete, the model will need to include temperature dependent thermal properties, two-dimensional heat flow, and shorter term precipitation rate changes. The model will very likely need to consider the effects of ice flow pattern and ice sheet thickness changes and recent movements of the ice divide. To determine the history of these last changes will require something beyond a pure heat flow model.

The heat flow at Summit does not happen in and by itself, rather it is coupled to the ice deformation of the Summit ice divide. An accurate model of the heat flow at Summit will probably have to be a coupled, thermo-mechanical model with heat and ice flow responding to past changes in precipitation rate and temperature. The physics of such a model is rather complex and non-linear. It needs to include the temperature and strain rate dependent power flow law for ice, the longitudinal stresses that appear near an ice divide, and a moving ice sheet surface. Such complex physics will demand more complex boundary conditions and boundary condition data; for example, the detailed surface and bedrock topography of the ice sheet, the surface strain rate and precipitation rate (mass balance) along the flow-line, age versus depth profiles, the ages and locations of prominent annual layers, and some sort of mass balance history applied far from the divide.

Such an intricate, time-dependent problem is ideally suited to optimal control methods. We could set up the heat flow control problem as before, introduce other forcings as controls (for example, the past precipitation rate), and manipulate these controls along with the past surface and basal flux. We could interpret the present day ice sheet profile and age versus depth relations as additional terminal constraints. We could introduce the physics of ice flow into the performance functions with additional Lagrange multipliers. We could then step the coupled ice and heat flow equations through time, compare the terminal results to the observations, run the adjoint model

to determine the gradients of the forcings, and then, as before, minimize until we find the forcings that best match the data.

Running such a complex model by control methods would be more costly. Obtaining a solution might require more boundary condition data than we can obtain. It is not clear to me if a complex model and solution are currently feasible. As a thought experiment, at least, constructing a sufficiently complete model and running it to a solution are both possible.

The Prospects for a Thorough Uncertainty Analysis The results, once we obtain them, will require a better uncertainty analysis than I have given here. The analysis can be provided by a straightforward computation of the Hessian as described in §7.3. The perturbation analysis calculating the Hessian will require work comparable to the minimizations obtaining a most likely solution. If we can construct a model and obtain a solution, we will be able to work an uncertainty analysis.

In summary, to distinguish the Younger Dryas event, we will need to obtain more accurate temperature observations, to construct and run a more accurate and complete model, and to perform a more thorough uncertainty analysis. An extensive study is needed to determine if these tasks can be accomplished. Thus there is still some prospect of distinguishing the Younger Dryas event from the borehole temperatures measured at Summit.

CHAPTER EIGHT

Summary and Conclusions

THE CONTROVERSY SURROUNDING the Younger Dryas event remains unresolved. The Greenland ice cores suggest an abrupt 7 K cooling between 11 500 and 10 700 yr B.P. We have still to determine how much of that cooling is real and how much might reflect isotopic meltwater "spikes." It is unclear then which explanation for the event is more plausible: Broecker's theory—supposing a large scale change in the North Atlantic ocean circulation and major cooling in Greenland—or Fairbanks's—supposing a reduced mixed layer, a tainted $\delta^{18}0$ record, and little or no cooling in Greenland.

8.1 Results and Prospects of Borehole Thermometry

Borehole thermometry has shown promise as an independent, direct geophysical method giving evidence that might resolve the controversy. With a simple heat flow model, "fast science" sensitivity analysis, and optimal control methods, the method has found best fits to the temperatures measured at Dye 3 and produced temperature histories for Greenland in agreement with the generally known changes in the Northern Hemisphere's past climate.

The method will require refinement before it can resolve the climate at the time of the Younger Dryas event. It needs more accurate observations, a better heat flow model, and a more refined uncertainty analysis. The GISP II and GRIP projects now underway at Summit, Greenland, will likely obtain a more accurate data set. Straightforward extensions of this work's finite element and finite difference methods will produce a better heat flow model. An analysis of the Hessian will extend this work's sensitivity tests and provide a refined uncertainty analysis.

Whether or not the method will be able to resolve the Younger Dryas event is a matter of time and information. To resolve such a short event, an analysis will need to reconstruct the past ice and heat flow at Summit in great detail. Such a reconstruction

will require a complex, thermomechanical model and detailed boundary condition data. The model will require large amounts of computer time.

8.2 Borehole Thermometry Worth Pursuing

Without further study, it is unclear if such an analysis is feasible, that is, whether sufficient computer time and observations will be forthcoming. Nevertheless, I think such an analysis is worth pursuing.

A Proxy for Past Changes The heat flow in an ice sheet does not happen in and by itself, rather it is coupled to the ice deformation within the ice sheet. This greatly complicates the task of resolving the past temperature signal from measured borehole temperatures. At the same time, the solutions obtained from borehole temperature analysis tell more about past conditions than just the past temperature. This should help the resolution of the Younger Dryas event: the recovery of other parameters will place the temperature changes during the Younger Dryas into better context.

The temperatures measured in a borehole are not a direct measure of past temperatures; rather, they are proxies for other parameters as well, such as past precipitation rate changes. Perhaps this is a weak argument for measuring and analyzing borehole temperatures. Chemical species measured in ice cores already serve as proxies, their record does not suffer strong diffusion, and they yield climate histories which are likely to be more detailed. It is unclear if thermal diffusion might not smear the Younger Dryas signal recorded in Greenland borehole temperatures and make it unrecognizable. Thus, there seems little point in pursuing a complicated analysis that will produce a fuzzier record and might never resolve the controversy.

It would be vain, however, to suppose the chemical species alone will best explain the past climate of Greenland. Their values as recorded in an ice core are the product of complicated, multi-stage processes. In contrast, the proxy temperature and precipitation records implied by a set of borehole temperatures result from simpler, more readily described, geophysical heat and ice flow. While it may lack detail, the climate record from borehole temperatures is a more direct proxy of its supposed forcings. This directness may allow borehole thermometry to determine and explain past climate obscured by complicating effects in the isotopic records. This directness may suggest the complicating effects in those records as well. Two examples suggested by the present work illustrate this.

Non-Temperature Effects in the Delta O-18 Record The $\delta^{18}0$ "paleo-thermometer" has not been calibrated except for changes happening over fairly recent times (e.g. Johnsen 1977). As discussed earlier (§4.13), it is probably unrealistic to assume that the observed present day relation between $\delta^{18}0$ value and mean annual air temperature in Greenland has held at all times. Figure 8.1 compares the recent surface temperature history determined from the 1983/1986 Dye 3 temperatures against the corrected $\delta^{18}0$ values obtained from the Dye 3 ice core. The figure plots the $\delta^{18}0$ values as the temperatures implied by one calibration of $\delta^{18}0$ paleo-thermometer. Between 5500 and 400 yr B.P., where the borehole temperature history is well-constrained, the two generally agree.

Even after 40~45 year averaging, the $\delta^{18}0$ values show considerable short term variations. From these values alone, it is not possible to determine if these are air temperature changes or the effects of some complication such as changes in precipitation source.

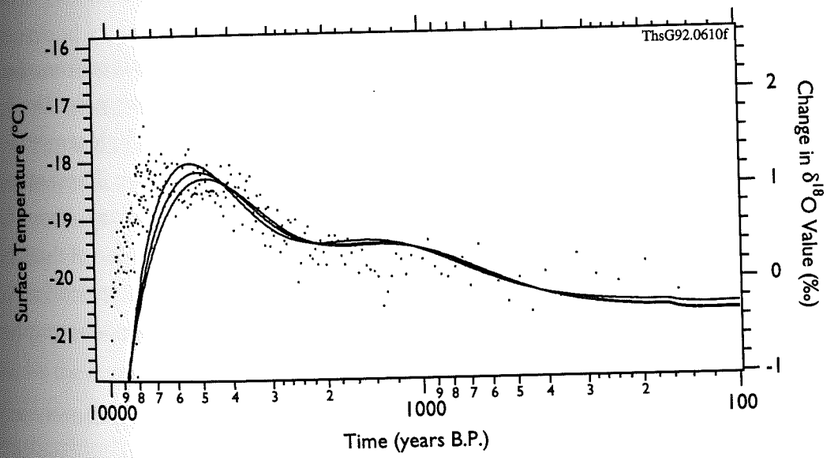

Fig. 8.1 The recent temperature history determined from the Dye 3 borehole temperatures (Fig. 6.8b) compared against corrected $\delta^{18}O$ values from the Dye 3 ice core (Fig. 4.5). Between 5500 and 400 yr B.P., the isotope values generally agree with the history implied by the Dye 3 borehole temperatures. Between these times, the values show short term variations which may or may not reflect changes in surface temperature.

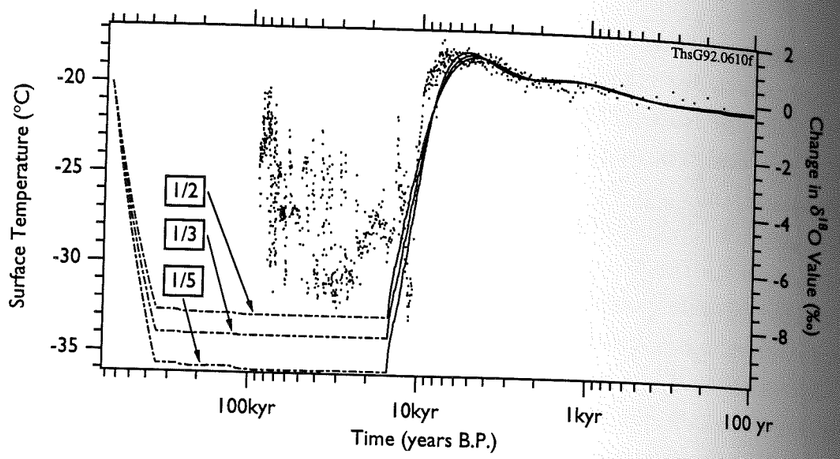

Fig. 8.2 *The older temperature history determined from the Dye 3 borehole temperatures (Fig. 6.8a) compared against corrected $\delta^{18}O$ values from the Dye 3 ice core (Fig. 4.5). The warmest ice age temperature suggested by the borehole temperatures is considerably colder than the average temperature implied by the $\delta^{18}O$ values.*

Figure 8.2 compares the older surface temperature history determined from the 1983/1986 Dye 3 temperatures against the older $\delta^{18}0$ values obtained from the Dye 3 ice core. Because diffusion has removed more rapid variations, the borehole temperatures can only suggest average air temperature values over the last ice age. These average values are considerably colder than the value implied by the $\delta^{18}0$ record. About 4 degrees of the difference is likely caused by the 2.5‰ increase in $\delta^{18}0$ value of the ice age ocean source water (Fig. 1.6). This leaves 2–5 degrees cooling unaccounted for. A number of hypotheses have been advanced for this failure of the $\delta^{18}0$ paleo-thermometer; for example, changes in the yearly distribution of precipitation.

A More Direct Proxy of Past Temperature Except for large, long-term precipitation rate changes, the borehole temperatures at Dye 3 are largely insensitive to such non-temperature effects. Thus, borehole thermometry can provide temperature histories more faithful to the past temperature in Greenland, especially over the last ice age when these non-temperature effects are most pronounced. The histories would show less detail because of greater thermal diffusion. In this example, however, the histories, as more

direct averages of past temperatures, would be free of the seasonal variations of precipitation that complicate the $\delta^{18}0$ record.

A Means to Isolate Non-Temperature Effects Borehole thermometry with a refined uncertainty analysis could identify the $\delta^{18}0$ variations that are consistent with the heat flow physics at Dye 3 and so determine which are temperature changes and which are something else. For more recent, short-term variations, the history determined from the borehole temperatures would be fairly detailed. Removing this temperature signal from the $\delta^{18}0$ values would leave a residual showing the magnitude and timing of these non-temperature effects. For older variations, the history would be an average of past changes. Removing this average would show the magnitude of long term effects.

By isolating the average magnitude of older changes or the magnitude and timing of more recent changes, a borehole temperature analysis could help determine the causes of these non-temperature effects.

The Pursuit of the "Holy Grail" The pronounced and rapid changes during the Younger Dryas have established the Younger Dryas event as perhaps the greatest unsolved problem of the last deglaciation. It has been argued that the changes in the Greenland ice cores that have been associated with the event result from a non-temperature effect. Testing this hypothesis is of great interest because it might prove or disprove several theories for the Younger Dryas.

The Younger Dryas event, though it is perhaps the most famous, is not the only problem of its kind. There are other important climatic problems that require answers for non-temperature effects; for example, the cold temperatures during the last ice age and the anomalously warm temperatures implied by the $\delta^{18}0$ values. As one geophysical modeler is fond of remarking, an explanation for the Younger Dryas controversy may prove to be the "holy grail" of climate research. Borehole thermometry may never resolve the controversy. However, if an impossible quest leads us to examine these other problems, then resolving the Younger Dryas event through borehole thermometry is worth trying, for no other reason than the answers we might encounter along the way.

APPENDICES
BIBLIOGRAPHY

APPENDIX A

Finite Element Model

THE TEMPERATURE WITHIN an ice sheet is determined by heat flow through a continuum. The heat flow can be modelled continuously in time and space by a system of partial differential equations and suitable boundary conditions. Except for very simple problems, however, finding an exact solution to the heat flow system can be difficult to impossible.

The finite element method is an approximation procedure that converts a problem expressed over a continuum to a tractable set of linear equations. In brief, the method breaks a problem over a large domain into a set of simpler problems over smaller finite pieces or elements. Within each element, the method assumes a simple variation for the solution. By piecewise integration over each element of the governing differential equations, the method obtains a solution at a set of nodes defined within the elements and along their boundaries. From these nodal values and the assumed variation within each element, the method then forms an approximate global solution.

The interested reader may consult Huebner (1982), Zienkiewicz (1977), or Zienkiewicz and Taylor (1989; 1991) for thorough treatments of the finite element method. Perhaps I can illustrate the method by applying it, step by step, to obtain the one-dimensional heat flow model described in Chapter 2. I will follow the approach of Huebner.

A.1 Discretize the Continuum

I solve for the temperature evolution at Dye 3 using a layered model of 2000 m of ice upon 3000 m of rock. For simplicity, I model the heat flow in a vertical line passing through the Dye 3 borehole. To apply the finite element method, I first subdivide the two layers into appropriate ice and rock elements. Since I am modelling heat flow along a line, the elements I use are a set of vertical line segments stretching from the surface into the bed, for example, as shown schematically in Figure 2.5.

A.2 Assume Simple Variations within the Elements

I assume that the fields vary quadratically within each of the one-dimensional elements. To represent these variations exactly, I assign three nodes within each element, one in the middle and at each end:

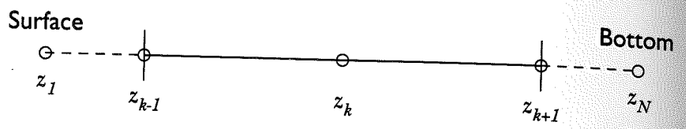

At the nodes, I assign values for each field variable (e.g. the temperature and vertical velocity). In between, I interpolate the values using

$$\phi(z) = \sum_{k=1}^{3} N_k(z)\,\phi_k. \tag{A.1}$$

The variables ϕ_k are the values at the nodes while N_k are the Lagrange interpolating polynomials through the nodes (Conte and De Boor 1980, §2.2) defined by:

$$N_k(z) = \prod_{\substack{i=1 \\ i\neq k}}^{3} \frac{z - z_k}{z_k - z_i}. \tag{A.2}$$

Graphically, the Lagrange polynomials look like:

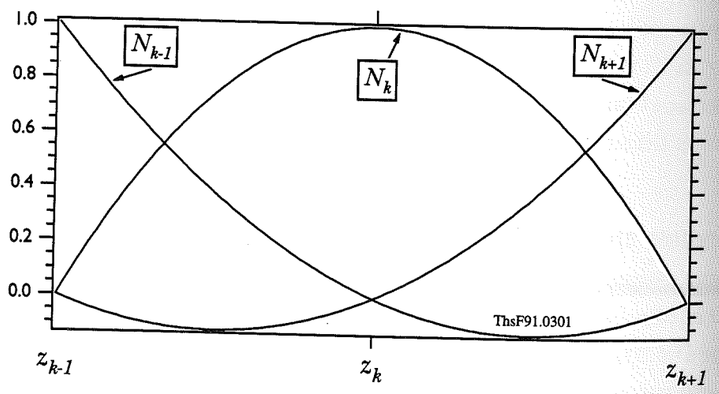

The polynomials are often called the "shape" functions for the element, because, as in the diagram, they give the shape of the interpolated fields.

A.3 Derive the Element Equations

I now derive the integral equations that the temperature field should satisfy within each element. For this step, I have several methods to choose from. To find a set of linear equations satisfying my differential equations and boundary conditions, I could use: the direct approach, the variational approach (Ritz method), the weighted residual approach, or the energy balance approach. I will follow the weighted residual approach.

The first step of the method, which I have already taken, is to assume that each field varies simply within each element. Having done this, it is now unlikely that the method can exactly satisfy the differential equations of my problem. There will likely be some residual between the exact solution of the heat flow equation and the solution using the simply-varying, field variable approximates. As the name implies, the method of weighted residuals tries to find an approximate solution to the differential equations that minimizes the weighted residual or error integrated over the entire solution domain.

There are a number of choices for the weighting. One popular choice and the one I shall use is the *Galerkin criterion,* which makes the weighting functions the same functions used to represent the field variables. Following this criterion, I require that the error satisfying the heat flow equations (2.6)–(2.8), weighted by the assumed variation for the temperature, vanish over each element. (If this is true, then the weighted error will also vanish over the entire solution domain.) If I define N_i as the Lagrange polynomials I use to approximate the temperature, over each element I require that

$$\int_V N_i \left[\rho c \frac{\partial T}{\partial t} - \frac{\partial}{\partial z} K \frac{\partial T}{\partial z} + \rho c u \frac{\partial T}{\partial x} + \rho c w \frac{\partial T}{\partial z} - f \right] dV = 0. \tag{A.3}$$

(The derivation in this appendix will assume heat flow that is mostly one-dimensional with a few two-dimensional corrections. By substituting suitable shape functions at this step and introducing a horizontal conduction term, this derivation may be applied to more general two-dimensional heat flow problems.)

A.4 Introduce Heat Flux Boundary Conditions

I wish to prescribe as a boundary condition, a fixed geothermal heat flux at the bed and, in some cases, a time-dependent flux forcing at the surface:

$$K\frac{\partial T}{\partial z}\bigg|_{\text{bed}} = Q_g \tag{A.4a}$$

$$K\frac{\partial T}{\partial z}\bigg|_{\text{sfc}} = Q_s(t) \tag{A.4b}$$

To introduce these conditions, I integrate (A.3) by parts

$$\int_V \rho c N_i \frac{\partial T}{\partial t} dV + \int_V \frac{\partial N_i}{\partial z} K \frac{\partial T}{\partial z} dV + \int_V N_i \rho c w \frac{\partial T}{\partial z} dV + \int_V N_i \left(\rho c u \frac{\partial T}{\partial x} - f \right) dV - \int_S N_i K \frac{\partial T}{\partial z} \cdot \hat{n} dS = 0 \tag{A.5}$$

where $\hat{n}$ is the unit normal to the surface S. The last term is the integrated surface flux added to the element by external sources. For interior elements, the last term is zero. At the surface and bed, its value is the integral of (A.4a) or (A.4b). After substituting these integrals and regrouping, I can write (A.5) as

$$\int_V \rho c N_i \frac{\partial T}{\partial t} dV + \int_V \left(\frac{\partial N_i}{\partial z} K + N_i \rho c w \right) \frac{\partial T}{\partial z} dV + \int_V N_i \left(\rho c u \frac{\partial T}{\partial x} - f \right) dV - Q = 0 \tag{A.6}$$

where

$$Q = \begin{cases} \int_S N_i Q_s(t) dS & \text{(for the surface element)} \\ 0 & \text{(for interior elements)} \\ \int_S N_i Q_g dS & \text{(for the bottom element)} \end{cases} \tag{A.7}$$

is the externally applied heat flux.

A.5 Assemble the Element Matrixes

I now derive the matrix equations that will express the behavior of the temperature field within each element. My objective will be to isolate in equation (A.6) the nodal temperatures and nodal temperature derivatives so that I may solve for them. Using (A.1), I can express the temperature throughout an element in terms of the temperature at its nodes,

$$T(z) = \sum_{j=1}^{3} N_j(z)\, T_j, \tag{A.8}$$

and, likewise, its temporal derivative,

$$\frac{\partial T}{\partial t}(z) = \sum_{j=1}^{3} N_j(z)\, \dot{T}_j. \tag{A.9}$$

Differentiating (A.8), I can find a similar expression for its spatial derivative,

$$\frac{\partial T}{\partial z}(z) = \sum_{j=1}^{3} \frac{\partial N_j(z)}{\partial z} T_j. \tag{A.10}$$

Substituting (A.8)–(A.10) into (A.6), I obtain

$$\int_V \left(\frac{\partial N_i}{\partial z} K + N_i \rho c w \right) \sum_{j=1}^{3} \frac{\partial N_j}{\partial z} T_j \, dV + \int_V \rho c N_i \sum_{j=1}^{3} N_j \dot{T}_j \, dV + \int_V N_i \left(\rho c u \frac{\partial T}{\partial x} - f \right) dV - Q = 0 \tag{A.11}$$

Changing the order of summation and integration, I can rewrite (A.11) in matrix form as

$$\mathbf{K}^e \mathbf{T}^e + \mathbf{C}^e \dot{\mathbf{T}}^e + \mathbf{R}^e - \mathbf{Q}^e = \mathbf{0}. \tag{A.12}$$

where I define the element's nodal temperatures, $\mathbf{T}^e$, its nodal temperature time derivatives, $\dot{\mathbf{T}}^e$, its conductivity matrix,

$$K_{ij}^e = \int_V \left(K \frac{\partial N_i}{\partial z} + \rho c w N_i \right) \frac{N_j}{\partial z} \, dV, \tag{A.13}$$

its heat capacity matrix,

$$C_{ij}^e = \int_V \rho c N_i N_j dV \,, \tag{A.14}$$

and its horizontal advection and strain heating nodal flux matrix,

$$R_i^e = \int_V N_i \left(\rho c u \frac{\partial T}{\partial x} - f \right) dV \,. \tag{A.15}$$

A.6 Approximate the Temperature Time Derivative ($\dot{\mathbf{T}}$)

I now have a set of linear equations for each element that includes the heat flow equations and their heat flux boundary conditions. These equations have the nodal temperatures and nodal temperature time-derivatives as unknowns. I could express the time derivative of the temperature as I have expressed its spatial derivatives. In a single step, I could then solve these equations for the unknown nodal temperatures at all times. Instead, I approximate the nodal temperature derivatives and solve the nodal temperatures over time using an implicit time-stepping scheme.

I approximate the temperature's time-derivative by the finite difference

$$\dot{\mathbf{T}}^e(t+\Delta t) = \frac{\mathbf{T}^e(t+\Delta t) - \mathbf{T}^e(t)}{\Delta t} \,. \tag{A.16}$$

I substitute this expression into (A.12) at time $t+\Delta t$ and obtain

$$\mathbf{K}^e(t+\Delta t)\mathbf{T}^e(t+\Delta t) + \mathbf{C}^e(t+\Delta t)\frac{\mathbf{T}^e(t+\Delta t) - \mathbf{T}^e(t)}{\Delta t} + \mathbf{R}^e(t+\Delta t) - \mathbf{Q}^e(t+\Delta t) = \mathbf{0} \,. \tag{A.17}$$

A.7 Combine the Element Matrixes

If I take time steps, $\Delta t(m)$, and I define $\mathbf{C}^e(m)$, $\mathbf{K}^e(m)$, $\mathbf{Q}^e(m)$, $\mathbf{R}^e(m)$, and $\mathbf{T}^e(m)$ as the heat capacity, heat conductivity, external heat flux, internal heat flux, and nodal temperature matrices at time $t(m)$,

$$t(m) = t_0 + \sum_{i=1}^{m} \Delta t(i) \,. \tag{A.18}$$

I can represent the heat flow in an element over each time step as

$$\mathbf{K}^e(m)\mathbf{T}^e(m) + \frac{\mathbf{C}^e(m)}{\Delta t(m)}\left\{\mathbf{T}^e(m) - \mathbf{T}^e(m-1)\right\} + \mathbf{R}^e(m) - \mathbf{Q}^e(m) = \mathbf{0} \,. \tag{A.19}$$

The field within each element is not independent, but is tied to its neighbors through shared nodes. At each shared node, the temperatures of two adjacent elements are equal and the heat flux is the sum of heat fluxes from each. This permits the individual element equations to be combined into a single set of global equations. These equations can then be solved simultaneously to obtain the temperatures at all the nodes.

If I denote $\mathbf{A}^k$ as the coefficient matrix, $\mathbf{A}^e$, from the *k-th* element and number the elements $1,\ldots,K$ (top-most to bottom-most), I can assemble a set of global coefficient matrices by the following procedure:

```
for k = 1,..., K do:
  for i = 1,2,3 do:
    for j = 1,2,3 do:
      C_(2k-2+i)(2k-2+j) = C^k_ij
      K_(2k-2+i)(2k-2+j) = K^k_ij
    end
    R_(2k-2+i) = R^k_i
  end
end
Q_1 = Q_s
Q_N = Q_g
```

(I have omitted time step indices for brevity.) With these coefficient matrixes and (A.19), I can write the global, nodal equations as

$$\mathbf{K}(m)\mathbf{T}(m) + \frac{\mathbf{C}(m)}{\Delta t(m)}\left\{\mathbf{T}(m) - \mathbf{T}(m-1)\right\} + \mathbf{R}(m) - \mathbf{Q}(m) = \mathbf{0} \,. \tag{A.20}$$

With external heat fluxes given by (A.7), in one dimension, and in scalar form, the nodal equations appear as

$$\begin{bmatrix} K_{11}^1 & K_{12}^1 & K_{13}^1 & 0 & 0 & . & . \\ K_{21}^1 & K_{22}^1 & K_{23}^1 & 0 & 0 & . & . \\ K_{31}^1 & K_{32}^1 & K_{33}^1 + K_{11}^2 & K_{12}^2 & K_{13}^2 & . & . \\ 0 & 0 & K_{21}^2 & K_{22}^2 & K_{23}^2 & . & . \\ 0 & 0 & K_{31}^2 & K_{32}^2 & K_{33}^2 + K_{11}^3 & . & . \\ . & . & . & . & . & . & . \\ 0 & 0 & 0 & 0 & 0 & . & K_{33}^N \end{bmatrix} \begin{bmatrix} T_1(m) \\ T_2(m) \\ . \\ . \\ . \\ . \\ T_N(m) \end{bmatrix}$$

$$+ \begin{bmatrix} C_{11}^1 & C_{12}^1 & C_{13}^1 & 0 & 0 & . & 0 \\ C_{21}^1 & C_{22}^1 & C_{23}^1 & 0 & 0 & . & 0 \\ C_{31}^1 & C_{32}^1 & C_{33}^1 + C_{11}^2 & C_{12}^2 & C_{13}^2 & . & 0 \\ 0 & 0 & C_{21}^2 & C_{22}^2 & C_{23}^2 & . & 0 \\ 0 & 0 & C_{31}^2 & C_{32}^2 & C_{33}^2 + C_{11}^3 & . & 0 \\ . & . & . & . & . & . & . \\ 0 & 0 & 0 & 0 & 0 & . & C_{33}^N \end{bmatrix} \begin{bmatrix} T_1(m) - T_1(m-1) \\ T_2(m) - T_2(m-1) \\ . \\ . \\ . \\ T_N(m) - T_N(m-1) \end{bmatrix} \Delta t(m)$$

$$+ \begin{bmatrix} R_1^1 \\ R_2^1 \\ R_3^1 + R_1^2 \\ . \\ . \\ R_2^N \\ R_3^N \end{bmatrix} - \begin{bmatrix} Q_s(m) \\ 0 \\ 0 \\ . \\ . \\ 0 \\ Q_g \end{bmatrix} = 0 \qquad \text{(A.21)}$$

where $N = 2K+1$ is the number of nodes.

Assembling these nodal equations can be quite tedious. I use a general purpose, finite element program to assemble and combine the element conductivity, heat capacity and heat flux matrixes into a set of global nodal equations (Zienkiewicz and Taylor 1989, c. 15).

A.8 Introduce Surface Temperature Boundary Conditions

In some cases, I wish to apply a surface temperature history to the model rather than a surface flux forcing. To do this, I ask the program to treat the temperature of the surface node as a fixed "displacement" and I supply its value at every time step. The program removes the surface temperature as an unknown from the nodal equations and substitutes these fixed values.

A.9 Solve the Time-Dependent Nodal Equations

Using the same finite element program, I solve for the time-varying temperature field between times $t(0)$ and $t(M)$ consistent with the initial and boundary conditions I specify. With a little rearranging, I produce from (A.20) an implicit relation between the temperature at times $t(m+1)$ and $t(m)$

$$\mathbf{T}(m) = \left\{\mathbf{K}(m) + \frac{\mathbf{C}(m)}{\Delta t(m)}\right\}^{-1} \cdot \left\{\frac{\mathbf{C}(m)}{\Delta t(m)}\mathbf{T}(m-1) - \mathbf{R}(m) + \mathbf{Q}(m)\right\}_{m=1,\ldots,M}. \qquad \text{(A.22)}$$

I start with an initial temperature field, $\mathbf{T}(0)$, fix a value for the basal flux, Q_g, and then in small time steps, $\Delta t(m)$, apply the program to solve (A.22) while varying the surface temperature or surface flux forcings, T_s or Q_s. The specific details of setting up and solving the time-dependent problem are provided in Zienkiewicz and Taylor (1991, c. 16).

A.10 Calculate the Terminal Model Temperatures

I step (A.22) through M time steps and obtain a set of terminal nodal temperatures, $\mathbf{T}(M)$. I wish to compare these against the present day Dye 3 temperature observations. Using the temperature shape functions (A.8), I reproduce the vertical temperature profile assumed by the heat flow model. From the N terminal nodal temperatures, I calculate terminal model temperature

$$\tilde{T}_n = \sum_{j=1}^{N} N_j(z_n) T_j(M) \qquad \text{(A.23)}$$

at each observation height, z_n.

APPENDIX B

A Better Time Mesh

THE HEAT FLOW MODEL described in Appendix A solves a discrete system of linear equations derived from the continuous heat transport equations. The time-stepped, model equations are unconditionally stable and *consistent* with the heat transport equations (Noye 1982): the model should agree with an exact solution to within a finite discretization error which approaches zero as the model's time step size decreases. Thus, the model can be stepped through time with a variable time step size.

B.1 Advantages of Lengthening the Time Steps

For three reasons, it is advantageous to step the model through time with a time step size that increases in size at earlier times.

B.11 More Efficient Heat Flow Modelling

The sensitivity tests of Chapter 3 imply that the temperatures in the Dye 3 borehole do not respond equally to the same surface temperature change applied at different times in the past. An older temperature change must last longer to produce an equally-strong response (Fig. 3.4). Thus, the surface temperature history we can determine from the Dye 3 borehole temperatures varies more slowly and shows less detail as we look further into the past.

To reproduce the evolution of the Dye 3 temperature fields at more recent times, the heat flow model requires small time steps, time steps that are needlessly small to reproduce the evolution at more ancient times. It is wasteful to take many small time steps where the climate changes slowly. The minimizations to obtain a solution demand many modelling runs; the computer time a run requires increases linearly with the number of time steps. By choosing a time step consistent with what I can reproduce of the past climate, I can reduce the computer time required by hours.

B.12 Better Minimization Performance

The surface temperature history we can determine from the Dye 3 borehole temperatures varies more slowly as we look further into the past. Equivalently, the Dye 3 borehole temperatures are less sensitive to more ancient temperature changes.

The variable metric minimization program finds a minimum by building up, iteratively, an approximation to the Hessian of the performance function. The speed at which the program converges to a minimum and the accuracy of its solution can decrease dramatically if the Hessian matrix becomes ill-conditioned, that is, its condition number approaches or exceeds the computer's round-off error (Gill *et al.* 1981). The Hessian can become ill-conditioned if a heat flow problem is poorly scaled, that is, the performance function varies much more rapidly with changes of certain parameters than with others.

The parameters I specify in later minimizations (c. 6 and 7) are the surface flux values at every time step and a geothermal heat flux value. According to Figure 3.4, at Dye 3 the duration of the shortest detectable surface temperature pulse varies by over five orders of magnitude between 675 000 and 100 yr B.P. If I use a fixed time step size, I can expect the sensitivity of the performance function with respect to the surface flux values to vary by a similar amount. The round-off error of the minimization program is on the order of 10^{-6}. With a fixed time step size, I can expect my problem will be poorly scaled. I can make it well scaled, and improve the performance of the minimization program by lengthening the time step size at earlier times

B.13 More Equal Regularization

The heat flow problem I wish to solve is ill-poised. To make its solution well-poised, I penalize its departure from a simple preconception: the (equivalent) surface flux histories and geothermal heat flux values determined in simple minimizations like those in §4.3. I define the penalty as the sum of the squared difference at each time step between the forcing solution and its preconception. I minimize this penalty to restrict the variation of the solution to no more than what is consistent with what may be determined from the Dye 3 borehole temperatures.

Since it is a sum of the differences at each time step, the size I choose for the time steps determines the variation I allow in the solution over each increment of time. To apply a consistent penalty and obtain the variation warranted over each time step, I should make the time steps I use in the heat flow model consistent with the variation I

may determine from the observations. The surface temperature history we can determine from the Dye 3 borehole temperatures varies more slowly as we look further into the past. By lengthening the time step at earlier times, I can make the regularization of the solution consistent with the observations.

B.2 Choosing Time Step Sizes

I choose model time step sizes consistent with the observations following a scheme that, in retrospect, is unnecessarily baroque. I first determine a modest number of time knots unequally-spaced in time so as to give surface temperature variations between each pair of time knots equal influence on the borehole temperatures. I then subdivide the time increments between knots in equally spaced increments until I have a sufficient number of model time steps to accurately model the past heat flow at Dye 3.

B.21 Choosing the Number of Time Knots

In §5.1, I suggested one way to regularize the heat flow solutions: make the surface temperature values at a few well chosen times the parameters in the minimizations, and then force the surface temperature to vary in a simple way at times in between. Following this approach, I would try to pick and place the fewest number of knots that explain the variations in the Dye 3 temperature observations.

Instead, in these solutions, I allow the surface temperatures greater variation and I then penalize their departure from a smooth preconception. Rather than pick and place the fewest number of knots that will explain the observations, I wish to pick and place a much greater number. I can estimate the number I will need by first determining what that fewest number might be.

The Fewest Number of Knots In the detailed heat flow model, I apply surface and basal heat flux forcings and obtain a set of terminal temperatures. Ultimately, I wish to find the forcings schedules that make the temperatures best match the data and that provide evidence for or against a Younger Dryas cooling. In the sensitivity test in §4.24, I found that a finite element mesh of 49 nodes was sufficient to model the past temperatures at Dye 3 to beyond the measured accuracy of the Dye 3 borehole temperatures.

The borehole observations that might show remnants of the Younger Dryas event lie between 0 and 1700 m height. Excluding the extra element I added near the ice

sheet bed to more accurately calculate strain heating, between these two heights there are a total of 21 nodes. With these 21 nodal values, I can expect to represent the effects of all the relevant temperature changes recorded in the Dye 3 temperature observations. I, therefore, can expect that I will be able to use no more than 21 independent values to represent the changes themselves, that is; in the model, I will be allowed no more than 21 independent parameters to represent the basal and surface heat flux forcings. Since the nodal temperature values are not linearly independent, I am not even allowed that number.

A Sufficient Number of Knots I expect the Dye 3 observations allow fewer than 21 degrees of freedom. To prevent the placement of the knots from significantly influencing the variation of the solution, I will place 101 time knots or roughly five times that number.

B.22 Placing the Time Knots

For the reasons given above, I wish to make the model time step sizes at different times consistent with the surface temperature variations I can determine from the Dye 3 borehole observations. From the sensitivity test of Chapter 3, I determined the shortest surface temperature pulse I should be able to detect in the present day Dye 3 borehole temperatures for times between 0 and 675 000 yr B.P. Since what I can not detect, I can not resolve, the results from this test suggest the shortest surface temperature changes I should seek at different times in the past.

Using the analysis of §3.24, I place the time knots so that a unit-amplitude surface temperature change at any of the knots has roughly the same effect on the present day borehole temperatures: that is, I space the knots so that a change at any of the knots yields a temperature response that just registers above some presumed noise level. Using trial and error, I vary the noise level until I obtain a total of 101 time knots between 0 and 675 000 yr B.P.

For each noise level, I compute a minimum detectable pulse width versus time curve as in Figure 3.4. I take the reciprocal of the curve's values, linearly interpolate in between, and then starting from time zero, I integrate to obtain a curve of accumulated sensitivity versus time. Starting from one end of the curve and working toward the other, I place time knots in increments of sensitivity equal to the noise level. When I finish, I count the number of knots I obtain. I adjust the noise level and repeat this procedure until I obtain exactly 101 time knots between 0 and 675 000 yr B.P.

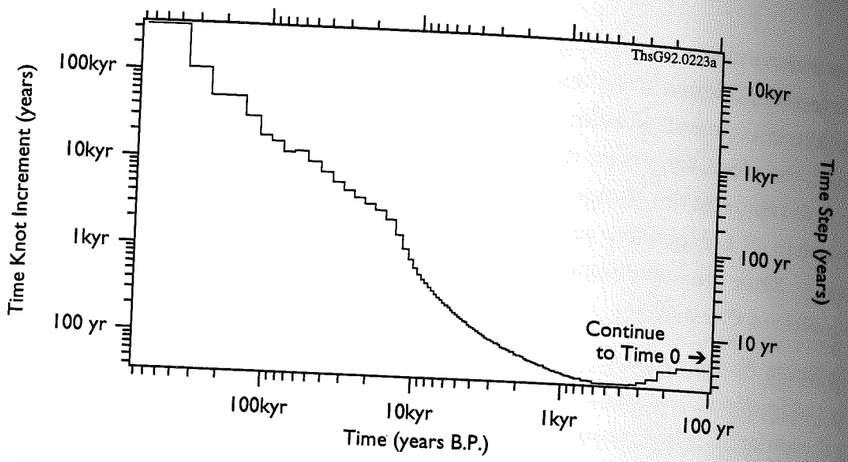

Fig. B.1 *The placement and sizes of the 101 knots and 1400 time steps that yield a maximum R.M.S. temperature error of 0.002 following a surface temperature step change. There is one more knot at time zero.*

Figure B.1 shows the placement and spacing of the surface flux time knots. To obtain 101 time knots, I require a noise level value, σ, of 0.0144.

B.23 Subdividing the Time Knots into Time Steps

These time knots are too far apart to step the heat flow model through time in 99 time steps: I need to subdivide the time steps in order to accurately model the heat flow at Dye 3. I subdivide each time step into n equal parts and I now determine what n should be. I follow a procedure somewhat like what I used to choose an efficient spatial mesh (§4.24).

I first subdivide the times between each pair of 101 time knots into a great many (2048) equal-size time steps. I fix the precipitation rate at today's value, apply a surface temperature step change, and step the heat flow model through time. I work from smaller steps to larger and at each of the 101 time knots, I save the borehole's temperature response. I gather together all the responses and call them the "true" temperature at those times. Next, I halve the number of time steps between each pair of knots and double their lengths, rerun the model, and obtain new sets of temperature values at each of the time knots. I compare these values against the "true" ones, calculate their root mean square difference, and find the maximum of the differences.

I repeat this procedure for successive time step halvings and record the maximum root mean square differences. From these, I estimate the number of time steps that will yield an acceptable maximum error at all times. Because I approximate the time derivative of temperature using a backward finite difference, and because the error of this approximation increases linearly with the time step size (Noye 1982; Press *et al.* 1986, c. 17), I relax the maximum error I will accept. I estimate the number of time steps that will yield a root mean square error roughly equal to the expected measurement error, 0.02 K, divided by the maximum surface temperature change, 10 K (i.e., an error of 1 part 500 or 0.002 K for a 1 K surface temperature change). Finally, I repeat this entire analysis to determine the number of steps required, assuming a typical ice age precipitation rate (1/3 today's value).

Table B.1 and Figure B.1 show the results. To obtain 1 part in 500 accuracy under both present day and ice age precipitation conditions, I require at least 14 intermediate time steps between each pair of time knots, or a total of 1400 time steps.

Table B.1 *Maximum Root Mean Square temperature error for the propagation of a surface temperature step change, as reproduced by the heat flow model run with different numbers of time steps and present day or ice age precipitation rates. The model requires roughly 1400 time steps to achieve an R.M.S. error of less than 0.002.*

Number of Timesteps	Maximum R.M.S. Error	
	Ppt Rate 0.53 m/a	Ppt Rate 0.17 m/a
100	0.015 0	0.011 5
200	0.009 71	0.005 93
400	0.005 77	0.003 02
800	0.003 22	0.001 52
1600	0.001 71	0.000 759
3200	0.000 878	0.000 377
6400	0.000 434	0.000 186

Bibliography

ALLEY, R.B. AND B.R. KOCI, 1990. Recent warming in Central Greenland? *Ann. Glaciol.*, **14**, 6–8.

BEER, J., M. ANDRÉE, H. OESCHGER, B. STAUFFER, R. BALZER, G. BONANI, C. STOLLER, M. SUTER, W. WÖLFLI, AND R.C. FINKEL, 1985. ^{10}Be variations in polar ice cores. *Geophysical Monograph No. 33*, American Geophysical Union, Washington D.C., 66–70.

BENFIELD, A.E., 1951. The temperature in an accumulating snowfield. *Monthly Notices of the Royal Astron. Soc., Geophys. Suppl.*, **6**(3), 139–147.

BOLZAN, J.F., 1985. Ice flow at the Dome C divide based on a deep temperature profile. *J. Geophys. Res.*, **90**(D5), 8111–8124.

BROECKER, W.S., 1990. Salinity history of the Northern Atlantic during the last deglaciation. *Paleoceanography*, **5**(4), 459–467.

BROECKER, W.S. AND G.H. DENTON, 1989. The role of ocean–atmosphere reorganizations in glacial cycles. *Geochimica et Cosmochimica Acta*, **53**, 2465–2501.

BROECKER, W.S., D.M. PETEET, AND D. RIND, 1985. Does the ocean–atmosphere system have more than one stable mode of operation? *Nature*, **315**, 21–26.

BROECKER, W.S., M. ANDREE, W. WOLFLI, H. OESCHGER, G. BONANI, J. KENNNETT, AND D. PETEET, 1988. The chronology of the last deglaciation: implications to the cause of the Younger Dryas event. *Paleoceanography*, **3**(1), 1–19.

BROECKER, W.S., J.P. KENNETT, B.P. FLOWER, J.T. TELLER, S. TRUMBORE, G. BONANI, AND W. WOLFLI, 1989. Routing of meltwater from the Laurentide Ice Sheet during the Younger Dryas cold episode. *Nature*, **341**, 318-321.

BROECKER, W.S., G. BOND, AND M. KLAS, 1990. A salt oscillator in the glacial Atlantic? 1. the concept. *Paleoceanography*, **5**(4), 469–477.

BUDD, W.F. AND N.W. YOUNG, 1983. Application of modelling techniques to measured profiles of temperatures and isotopes. *In* Robin, G. de Q., ed. *The Climatic Record in Polar Ice Sheets*. Cambridge University Press, New York, 150-177.

BRYSON, A.E. AND Y.-C. HO, 1975. *Applied optimal control: optimization, estimation, and control*. Halsted Press, New York, etc.

BRYAN, K.S. AND M.D. COX., 1968. A non-linear model of an ocean driven by wind and differential heating, parts I and II. *J. Atmospheric Sci.*, **25**, 945–978.

CLAUSEN, H.B. AND C.U. HAMMER, 1988. The Laki and Tambora eruptions as revealed in Greenland ice cores from 11 locations. *Ann. Glaciol.*, **10**, 16–22.

CLAUSEN, H.B., N.S. GUNDESTRUP, S.J. JOHNSEN, R. BINDSCHADLER, AND J. ZWALLY, 1988. Glaciological investigations in the Crête area, Central Greenland. *Ann. Glaciol.*, **10**, 10-15.

CLEVELAND, W.S., 1985. *The elements of graphing data*. Pacific Grove California, Wadsworth Advance Book Program.

CLIMAP PROJECT MEMBERS, 1981. Seasonal reconstruction of the Earth's surface at the last glacial maximum. *Geol. Soc. Am. Map Chart Ser.*, **36**.

CONSTABLE, S.C., R.L. PARKER, AND C.G. CONSTABLE, 1986. Occam's inversion: a practical algorithm for generating smooth models from electromagnetic sounding data. *Geophysics*, **52**, 289–300.

CONTE, S.D. AND C. DE BOOR, 1980. *Elementary numerical analysis.: an algorithmic approach*. New York, etc., McGraw-Hill Book Company.

DAHL-JENSEN, D., 1989. Steady thermomechanical flow along two-dimensional flow lines in large grounded ice sheets. *J. Geophys. Res.*, **94**(B8), 10 355–10 362.

———, 1991. Conversation with author, 22 April 1991.

DAHL-JENSEN, D. AND S.J. JOHNSEN, 1986. Palaeotemperatures still exist in the Greenland ice sheet. *Nature*, **320**(20), 250–252.

DANSGAARD, W., 1961. The isotopic composition of natural waters. *Medd. om Grønland*, **165**(2), 1–120.

DANSGAARD, W. AND S.J. JOHNSEN, 1969. A flow model and a time scale for the ice core from Camp Century, Greenland. *J. Glaciol.*, **8**(53), 215–223.

DANSGAARD, W. AND H. OESCHGER, 1989. Past environmental long-term records from the Arctic. *In* Oeschger, H. and C.C. Langway, Jr., eds. *The Environmental Record in Glaciers and Ice Sheets*. Wiley and Sons, 287–317.

DANSGAARD, W., S.J. JOHNSEN, H.B . CLAUSEN, C.U. HAMMER, AND N. GUNDESTRUP, 1973. Stable isotope glaciology. *Medd. om Grønland*, **197**(2), 1–53.

DANSGAARD, W., H.B. CLAUSEN, N. GUNDESTRUP, C.U. HAMMER, S.F. JOHNSEN [*sic?*], P.M. KRISTINSDOTTIR, AND N. REEH, 1982. A new Greenland deep ice core, *Science*, **218**, 1273–1277.

DANSGAARD, W., S.J. JOHNSEN, H.B. CLAUSEN, D. DAHL-JENSEN, N. GUNDESTRUP, AND C.U. HAMMER, 1984a. North Atlantic climatic oscillations revealed by deep Greenland cores. *Geophysical Monograph No. 29*, American Geophysical Union, 288–298.

DANSGAARD, W., H.B. CLAUSEN, D. DAHL-JENSEN, N. GUNDESTRUP AND C.U. HAMMER, 1984b. Climatic history from ice core studies in Greenland: data correction procedures. *In* Ghazi

A. and R. Fantechi, eds. *Current issues in climate research: proceedings of the European Community Climatology Programme Symposium.* D. Reidel Publishing Co., Boston, 45–60.

Dansgaard, W., H.B. Clausen, N. Gundestrup, S.J. Johnsen, and C. Rygner, 1985. Dating and climatic interpretation of two deep Greenland ice cores. *Geophysical Monograph No. 33,* American Geophysical Union, Washington D.C., 71–76.

Dansgaard, W., J.W.C. White, and S.J. Johnsen, 1989. The abrupt termination of the Younger Dryas climate event. *Nature,* **339**, 532–534.

Delmas, R.J. and M. Legrand, 1989. Long-term changes in the concentrations of major chemical compounds (soluble and insoluble) along deep ice cores. *In* Oeschger, H. and C.C. Langway, Jr., eds. *The Environmental Record in Glaciers and Ice Sheets.* Wiley and Sons, 319–341.

Emiliani, C., C. Rooth, and J.J. Stipp, 1978. The late Wisconsin flood into the Gulf of Mexico. *Earth Planet Sci. Let.,* **41**, 159–162.

Fairbanks, R.G., 1989. A 17,000-year glacio-eustatic sea level record: influence of glacial melting rates on the Younger Dryas event and deep-ocean circulation. *Nature,* **342**, 637–642.

Finkel, R.C. and C.C. Langway, Jr., 1985. Global and local influence on the chemical composition of snowfall at Dye 3, Greenland. *Earth Planet Sci. Let.,* **73**, 196–206.

Firestone, J., E. Waddington, and J. Cunningham, 1990. The potential for basal melting under Summit, Greenland: the record between 10 ka B.P. and 40 ka B.P. *J. Glaciol.,* **36**(123), 163–168.

Fisher, D.A., N. Reeh, and H.B. Clausen, 1985. Stratigraphic noise in time series derived from ice cores. *Ann. Glaciol.,* **7**, 76–83.

Gill, P.E., W. Murray, and M.H. Wright, 1981. *Practical Optimization.* Academic Press, London, etc.

Glen, J.W., 1958. The flow law of ice: a discussion of the assumptions made in glacier flow theory, their experimental foundations and consequences. *Publ. No. 47,* Int. Assn. of Hydrological Sciences, IUGG, Symposium of Grenoble, 171-183.

Gundestrup, N.S., 1991. Conversation with author, 24 April 1991.

Gundestrup, N.S. and B.L. Hansen, 1984. Bore-hole survey at Dye 3, South Greenland. *J. Glaciol.,* **30**(106), 282–288.

Gundestrup, N.S., S.J. Johnsen, and N. Reeh, 1984. ISTUK: a deep ice core drill system. *CRREL Special Report,* **83-34**, 7–19.

Gundestrup, N.S., D. Dahl-Jensen, B.L. Hansen, and J. Kelty, unpublished. Bore-hole survey at Camp Century, 1989.

Gundestrup, N.S., D. Dahl-Jensen, S.J. Johnsen, B.L. Hansen, and A. Rossi., unpublished. Borehole survey at Dome Grip 1991. *Submitted to Cold Reg. Sci. Technol.*

Hammer, C.U., 1989. Dating by physical and chemical seasonal variations and reference horizons. *In* Oeschger, H. and C.C. Langway, Jr., eds. *The Environmental Record in Glaciers and Ice Sheets.* Wiley and Sons, 99–121.

Hammer, C.U., H.B. Clausen, W. Dansgaard, A. Neftel, P. Kristinsdottir, and E. Johnson, 1985. Continuous impurity analysis along the Dye 3 deep core. *Geophysical Monograph No. 33,* American Geophysical Union, Washington, D.C., 90–94.

Hammer, C.U., H.B. Clausen, and H. Tauber, 1986. Ice-core dating of the Pleistocene/Holocene boundary applied to a calibration of the ^{14}C time scale. *Radiocarbon,* **28**(2A), 284–291.

Hammer, C.U., H.B. Clausen, W.L. Friedrich, and H. Tauber, 1987. The Minoan eruption of Santorini in Greece dated to 1645 BC? *Nature,* **328**, 517–519.

Hansen, B.L. and N.S. Gundestrup, 1988. Resurvey of bore hole at Dye 3, South Greenland. *J. Glaciol.,* **34**(117), 178–182.

Herron, S. and C.C. Langway, 1985. Chloride, nitrate, and sulfate in the Dye 3 and Camp Century, Greenland ice cores. *Geophysical Monograph No. 33,* American Geophysical Union, Washington D.C., 77–84.

Hooke, R.L., C.A. Alexander, and R.J. Gustafson, 1980. Temperature profiles in the Barnes Ice Cap, Baffin Island, Canada, and heat flux from the subglacial terrane. *Can. J. Earth Sci.,* **17**, 1174–1188.

Huebner, K.H., 1982. *The finite element method for engineers.* John Wiley and Sons, New York, etc.

Hutter, K., 1983. *Theoretical glaciology: material science of ice and the mechanics of glaciers and ice sheets.* Dordrecht, etc., D. Reidel Publishing Company.

Johnsen, S. J., 1977. Stable isotope profiles compared with temperature profiles in firn and with historical temperature records. *Publ. No. 118,* International Assn. of Hydrological Sciences, IUGG, Symposium of Grenoble, 388–392.

Johnsen, S.J., W. Dansgaard, and J.W.C. White, 1989. The origin of Arctic precipitation under present and glacial conditions. *Tellus,* **41B**, 452–468.

Koch, J.P. and A. Wegener, 1930. Wissenschaftliche Ergebnisse der dänische Expedition nach Dronning Louises-Land und quer über das Indlandeis von Nordgrön-land 1912–13 unter Leitung von Hauptmann J. P. Koch. *Medd. om Grønland,* **75**, 191–243.

Lamb, H.H., 1982. *Climate history and the modern world.* Methuen, London, etc.

Lawson, C.L. and R.J. Hanson, 1974. *Solving least squares problems.* Prentice Hall, Englewood Cliffs, New Jersey.

Le Roy Ladurie, E., 1971. *Times of feast, times of famine.* Noon Day Press, New York.

Letréguilly, A., N. Reeh, and P. Huybrechts, 1991. The Greenland ice sheet through the last glacial–interglacial cycle. *Palaeogeogr., Palaeoclimatol., Palaeoecol.,* **90**, 385–394.

LEVENBERG, K., 1944. A method for the solution of certain non-linear problems in least squares. *Q. Appl. Math.*, **2**, 164–168.

LEVENTER, A., D.F. WILLIAMS, AND J.P. KENNETT, 1982. Dynamics of the Laurentide ice sheet during the last deglaciation: evidence from the Gulf of Mexico. *Earth Planet Sci. Let.*, **59**, 11–17.

LORIUS, C., G. LAMBERT, R. HAGEMANN, L. MERLIVAT, AND J. RAVOIR, 1970. Dating of firn layers in Antarctica: application to the determination of the rate of snow accumulation. *Publ. No. 86,* International Assn. of Hydrological Sciences and Sci. Comm. on Antarctic Res., Proc. of Int. Symp. on Antarctic Glaciological Exploration, Hanover, N.H., 3–15.

MACAYEAL, D.R., J. FIRESTONE, AND E. WADDINGTON, 1991. Paleothermometry by control methods. *J. Glaciol.*, **37**(127), 326–338.

MANGERUD, J., 1980. Ice–front variations of different parts of the Scandinavian ice sheet, 13,000–10,000 years B.P. *In* Lowe, J.J., J.M. Gray, and J.E. Robinson, eds. *Studies in Late Glacial of North-West Europe.* Pergamon Press, Oxford, 23–30.

MARQUADT, D.W., 1963. An algorithm for least squares estimation for non-linear parameters. *J. Soc. Ind. Appl. Math.*, **11**, 431–441

MENKE, W., 1989. *Geophysical data analysis: discrete inverse theory.* Academic Press, San Diego, etc.

MORSE, P.M. AND H. FESHBACH, 1953. *Methods of theoretical physics.* McGraw-Hill, New York, etc.

NOYE, J., 1982. Finite difference methods for partial differential equations. *In* Noye, J., ed. *Numerical solutions of partial differential equations: proceedings of the 1981 Conference held at Queen's College, Melbourne University, Australia.* North-Holland Publishing Company, Amsterdam, etc., 3–138.

NYE, J.F., 1963. Correction factor for accumulation measured by the thickness of the annual layers in an ice sheet. *J. Glaciol.*, **4**(36), 785–788.

OESCHGER, H., J. BEER, U. SIEGENTHALER, B. STAUFFER, W. DANSGAARD, AND C.C. LANGWAY, 1984. Late glacial climate history from ice cores. *Geophysical Monograph No. 29,* American Geophysical Union, Washington D.C., 299–306.

OVERGAARD, S. AND N.S. GUNDESTRUP, 1984. Bedrock topography of the Greenland ice sheet in the Dye 3 area. *In* Oeschger, H. and C.C. Langway, Jr., eds. *The Environmental Record in Glaciers and Ice Sheets.* Jr. Wiley and Sons, 49-56.

PATERSON, W.S.B. AND G.K.C. CLARKE, 1978. Comparison of theoretical and observed temperature profiles in Devon Island ice cap, Canada. *Geophys. J. R. Astr. Soc.*, **55**, 615–632.

PATERSON, W.S.B., 1981. *The physics of glaciers, second edition.* Pergamon Press, Oxford, etc.

PATERSON, W.S.B. AND C.U. HAMMER, 1987. Ice core and other glaciological data. *In* Ruddimen, W.F. and H.E. Wright, Jr., eds. *North America and Adjacent Oceans during the last Deglaciation,* Geol. Soc. Am., 91–109.

PATERSON, W.S.B. AND E.D. WADDINGTON, 1986. Estimated basal ice temperatures at Crête, Greenland, throughout a glacial cycle. *Cold Reg. Sci. Technol.*, **12**, 99–102.

PHILIPS, B.L., 1962. A technique for the numerical solution of certain integral equations of the first kind. *J. Assoc. Comp. Mach.*, **9**, 84–97.

PICCIOTTO, E.E., X. DE MAERE AND I. FRIEDMAN, 1960. Isotopic composition and temperature of formation of Antarctic snows. *Nature,* **187**, 857–859.

PRESS, W.H., B.P. FLANNERY, S.A. TEUKOLSKY, AND W.T. VETTERLING, 1986. *Numerical recipes: the art of scientific computing.* Cambridge University Press, New York.

RAYMOND, C.F., 1983. Deformation in the vicinity of ice divides. *J. Glaciol.*, **29**(103), 357–373.

REEH, N., 1984. Reconstruction of the glacial ice covers of Greenland and the Canadian Arctic islands by three-dimensional, perfectly plastic ice-sheet modelling. *Ann. Glaciol.*, **5**, 115–121.

———, 1989a. The age–depth profile in the upper part of a steady-state ice sheet. *J. Glaciol.*, **35**(121), 406–417.

———, 1989b. Dating by ice flow modelling: a useful tool or an exercise in applied mathematics? *In* Oeschger, H. and C.C. Langway, Jr., eds. *The Environmental Record in Glaciers and Ice Sheets.* Wiley and Sons, 141–159.

———, 1990. Past changes in precipitation rate and ice thickness as derived from age–depth profiles from ice sheets: application to Greenland and Canadian Arctic ice-core records. *In* Bleil, U. and J. Thiede, eds. *Geologic history of the polar oceans: Arctic vs. Antarctic.* Dordrecht, Kluwer Academic Publishers, 255-271.

REEH, N., S.J. JOHNSEN, AND D. DAHL-JENSEN, 1985. Dating the Dye 3 deep ice core by flow model calculations. *Geophysical Monograph No. 33,* American Geophysical Union, Washington D.C., 57–65.

RITZ, C., 1987. Time dependent boundary conditions for calculation of temperature fields in ice sheets. *Int. Assn. of Hydrological Sciences Publication 170* (Symposium at Vancouver 1987—*The Physical Basis of Ice Sheet Modelling*), 207–216.

———, 1989. Interpretation of the temperature profile measured at Vostok, East Antarctica. *Ann. Glaciol.*, **12**, 138–144.

ROBIN, G. DE Q., 1955. Ice movement and temperature distribution in glaciers and ice sheets. *J. Glaciol.*, **2**(18), 523–532.

ROOTH, C., 1982. Hydrology and ocean circulation. *Prog. Oceanogr.*, **11**, 131–149.

RUDDIMAN, W.F., 1987. Northern Oceans. *In* Ruddimen, W.F. and H.E. Wright, Jr., eds. *North America and Adjacent Oceans during the last Deglaciation,* Geol. Soc. Am., 137–154.

RUSSELL, B., 1972. *A history of western philosophy.* Simon and Schuster, New York.

SCHØTT, C., E.D. WADDINGTON, AND C.F. RAYMOND, 1992. Predicted time scales for GISP2 and GRIP boreholes at Summit, Greenland. *J. Glaciol.*, **38**(128), 162–168.

SHACKLETON, N.J., 1967. Oxygen isotope analyses and Pleistocene temperatures, re-assessed. *Nature*, **215**, 15–17.

SCHNEIDER, S.H., D.M. PETEET, AND G.R. NORTH, 1987. A climate model intercomparison for the Younger Dryas and its implications for paleoclimatic data collection. *In* Berger, W.H. and L.D. Labeyrie, eds. *Abrupt Climate Change.* D. Reidel, 399–417.

SMITH, J.T. AND J.R. BOOKER, 1988. Magnetotelluric inversion for minimum structure. *Geophysics,* **53**(12), 1565–1576.

STOMMEL, H., 1961. Thermohaline convection with two stable regimes of flow. *Tellus,* **13**(2), 224–230.

SVERDRUP, H.U., 1935. Scientific results of the Norwegian Spitsbergen expedition in 1934. *Geografiska Annaler,* **17**, 53–88.

TARANTOLA, A., 1987. *Inverse problem theory: methods for data fitting and model parameter estimation.* Elsevier, Amsterdam.

TAYLOR, J.R., 1982. *An introduction to error analysis: the study of uncertainties in physical measurement.* University Science Books, Mill Valley, California.

TELLER, J.T., 1985. Glacial Lake Agassiz and its influence on the Great Lakes. *In* Karrow, P.F. and P.E. Calkin, eds. *Quaternary Evolution of the Great Lakes, spec. pap. 30.* Geological Assoc. of Canada, Ottawa, 1–16.

THACKER, W.C., 1988. Fitting models to inadequate data by enforcing spatial and temporal smoothness. *J. Geophys. Res.,* (**93**)C9, 10 655–10 665.

———, 1989. The role of the hessian matrix in fitting models to measurements. *J. Geophys. Res.,* (**94**)C5, 6177–6196.

THACKER, W.C. AND R.B. LONG, 1988. Fitting dynamics to data. *J. Geophys. Res.,* (**93**)C2, 1227–1240.

TWOMEY, S., 1962. On the numerical solution of Fredholm integral equations of the first kind by the inversion of the linear system produced by quadrature. *J. Assoc. Comp. Mach.,* **10**, 97–101.

———, 1965. The application of numerical filtering to the solution of integral equations encountered in indirect sensing measurements. *J. Franklin Inst.,* **279**(2), 95–109.

WADDINGTON, E.D., 1987. Geothermal heat flux beneath ice sheets. *Int. Assn. of Hydrological Sciences Publication 170* (Symposium at Vancouver 1987—*The Physical Basis of Ice Sheet Modelling*), 217–226.

WATTS, W.A., 1980. Regional variation in the response of vegetation to late glacial climatic events in Europe. *In* Gray, J.M. and J.E. Robinson, eds. *Studies in the Late Glacial Climatic Events in Europe.* Pergamon Press, Oxford, 1–21.

WEBER, C.F., 1981. Analysis and solution of the ill-poised inverse heat conduction problem. *Int. J. Heat Transfer,* **24**(11), 1783–1792.

WEERTMAN, J., 1968. Comparison between measured and theoretical temperature profiles of the Camp Century, Greenland, borehole. *J. Geophys. Res.,* **73**(8), 2691–2700.

WDC-A. *Dye 3 delta oxygen-18 versus depth, University of Copenhagen.* Boulder, WDC-A for Glaciology/National Snow and Ice Data Center, CIRES, Univ. of Colorado.

YEN, Y.-C., 1981. Review of critical properties of snow, ice, and sea ice. *CRREL Rep.* 81-10.

ZIENKIEWICZ, O.C., 1977. *The finite element method. Third edition.* London, etc., McGraw-Hill Book Company.

ZIENKIEWICZ, O.C. AND R.L. TAYLOR,1989. *The finite element method. Fourth edition, volume 1.* London, etc., McGraw-Hill Book Company.

———, 1991. *The finite element method. Fourth edition, volume 2.* London, etc., McGraw-Hill Book Company.